EBioMedicine 60 (2020) 102989

Contents lists available at ScienceDirect

EBioMedicine

journal homepage: www.elsevier.com/locate/ebiom

Research paper

Cell motility and migration as determinants of stem cell efficacy

Lusine Danielyan[a,b,*], Matthias Schwab[a,b,c,d], Georg Siegel[e], Bianca Brawek[f], Olga Garaschuk[f], Nithi Asavapanumas[f], Marine Buadze[a], Ali Lourhmati[a], Hans-Peter Wendel[g], Meltem Avci-Adali[g], Marcel A. Krueger[h], Carsten Calaminus[h], Ulrike Naumann[i], Stefan Winter[c], Elke Schaeffeler[c], Annett Spogis[a], Sandra Beer-Hammer[j], Jonas J. Neher[k,l], Gabriele Spohn[m], Anja Kretschmer[m], Eva-Maria Krämer-Albers[n], Kerstin Barth[n], Hong Jun Lee[o,p], Seung U. Kim[q], William H. Frey II[r], Claus D. Claussen[s], Dirk M. Hermann[t], Thorsten R. Doeppner[t,u], Erhard Seifried[m], Christoph H. Gleiter[a], Hinnak Northoff[e], Richard Schäfer[e,m,**]

[a] Department of Clinical Pharmacology, University Hospital Tübingen, Tübingen, Germany
[b] Neuroscience Laboratory and Departments of Biochemistry and Clinical Pharmacology, Yerevan State Medical University, Yerevan, Armenia
[c] Dr. Margarete Fischer-Bosch Institute of Clinical Pharmacology, Stuttgart, Germany and University of Tübingen, Tübingen, Germany
[d] Department of Pharmacy and Biochemistry, University of Tübingen, Tübingen, Germany
[e] Institute of Clinical and Experimental Transfusion Medicine, University Hospital Tübingen, Tübingen, Germany
[f] Institute of Physiology, Department of Neurophysiology, University of Tübingen, Tübingen, Germany
[g] Department of Thoracic, Cardiac and Vascular Surgery, University Hospital Tübingen, Tübingen, Germany
[h] Werner Siemens Imaging Center, Department of Preclinical Imaging and Radiopharmacy, University Hospital Tübingen, Tübingen, Germany
[i] Hertie Institute for Clinical Brain Research and Center Neurology, Department of Vascular Neurology, Tübingen Neuro-Campus (TNC), University of Tübingen, Tübingen, Germany
[j] Department of Pharmacology, Experimental Therapy and Toxicology, Institute of Experimental and Clinical Pharmacology and Pharmacogenomic, and ICePhA, University Hospital Tübingen, Tübingen, Germany
[k] Department of Cellular Neurology, Hertie Institute for Clinical Brain Research, University of Tübingen, Tübingen, Germany
[l] German Center for Neurodegenerative Diseases (DZNE), Tübingen, Tübingen, Germany
[m] Institute for Transfusion Medicine and Immunohematology, German Red Cross Blood Donor Service Baden-Württemberg-Hessen gGmbH, Goethe-University Hospital, Frankfurt am Main, Germany
[n] Institute for Developmental Biology and Neurobiology, Johannes Gutenberg University Mainz, Mainz, Germany
[o] College of Medicine and Medical Research Institute, Chungbuk National University, Cheongju, Chungbuk, Republic of Korea
[p] Research Institute eBiogen Inc., Seoul, Republic of Korea
[q] Division of Neurology, Department of Medicine, UBC Hospital, University of British Columbia, Vancouver, BC, Canada
[r] HealthPartners Center for Memory and Aging, HealthPartners Neurosciences, St. Paul, MN, U.S.A.
[s] Department of Radiology, University Hospital Tübingen, Tübingen, Germany
[t] Department of Neurology, University of Duisburg-Essen, Essen, Germany
[u] Department of Neurology, University Medical Center Göttingen, Göttingen, Germany

ARTICLE INFO

Article History:
Received 14 April 2020
Revised 13 August 2020
Accepted 20 August 2020
Available online 10 September 2020

Keywords:
Mesenchymal stem cells
Neural stem cells
Intranasal
Alzheimer's disease
Oncovirolysis

ABSTRACT

Background: Stem cells` (SC) functional heterogeneity and its poorly understood aetiology impedes clinical development of cell-based therapies in regenerative medicine and oncology. Recent studies suggest a strong correlation between the SC migration potential and their therapeutic efficacy in humans. Designating SC migration as a denominator of functional SC heterogeneity, we sought to identify highly migrating subpopulations within different SC classes and evaluate their therapeutic properties in comparison to the parental non-selected cells.

Methods: We selected highly migrating subpopulations from mesenchymal and neural SC (sMSC and sNSC), characterized their features including but not limited to migratory potential, trophic factor release and transcriptomic signature. To assess lesion-targeted migration and therapeutic properties of isolated subpopulations in vivo, surgical transplantation and intranasal administration of MSCs in mouse models of glioblastoma and Alzheimer's disease respectively were performed.

* Corresponding author at: Department of Clinical Pharmacology, University Hospital Tübingen, Auf der Morgenstelle 8, 72076 Tübingen, Germany.
** Corresponding author at: Institute for Transfusion Medicine and Immunohaematology, German Red Cross Blood Donor Service Baden-Württemberg-Hessen gGmbH, Sandhofstrasse 1, 60528 Frankfurt am Main, Germany.
E-mail addresses: lusine.danielyan@med.uni-tuebingen.de (L. Danielyan), richard.schaefer.md@gmail.com (R. Schäfer).

https://doi.org/10.1016/j.ebiom.2020.102989

Glioblastoma

Findings: Comparison of parental non-selected cells with isolated subpopulations revealed superior motility and migratory potential of sMSC and sNSC in vitro. We identified podoplanin as a major regulator of migratory features of sMSC/sNSC. Podoplanin engineering improved oncovirolytic activity of virus-loaded NSC on distantly located glioblastoma cells. Finally, sMSC displayed more targeted migration to the tumour site in a mouse glioblastoma model and remarkably higher potency to reduce pathological hallmarks and memory deficits in transgenic Alzheimer's disease mice.
Interpretation: Functional heterogeneity of SC is associated with their motility and migration potential which can serve as predictors of SC therapeutic efficacy.
Funding: This work was supported in part by the Robert Bosch Stiftung (Stuttgart, Germany) and by the IZEPHA grant.

Research in context

Evidence before this study

Current cell-based therapies have demonstrated therapeutic efficacy and broad applicability in treatment of degenerative and malignant brain disorders. Despite remarkable regenerative potential of stem cells in degenerated tissues and their tumour tropism used for oncovirolytic therapy, stem cell candidates show high variability in their therapeutic efficacies. Cell motility is one of the features that may substantially contribute to stem cell functional heterogeneity via its impact on cell homing to degenerated or tumour-affected tissue. Therefore, we tested our hypothesis on the existence of subpopulations with distinct cell motility and migratory properties within one stem cell entity using different stem cell types and models of central nervous system disorders.

Added value of this study

This study investigated the importance of stem cell motility and migration properties for their targeted homing to the degenerated or tumour-affected brain tissue in vitro and in vivo. Highly migrating subpopulations of mesenchymal and neural stem cells (MSC and NSC) were isolated from original murine and human cell populations respectively. In comparison to the non-selected parental cells, mesenchymal (sMSC) showed remarkably greater motility in vitro and higher potency to reach the degenerated brain tissue after intranasal administration in a transgenic mouse model of Alzheimer's disease. This feature strongly correlated with their therapeutic properties reflected by improved memory, neurogenesis, synaptogenesis, neuronal survival, amyloid beta clearance and by decreased cortical neuronal hyperactivity. In a model with stereotactic implantation of mouse glioblastoma, contralaterally transplanted sMSC have reached the tumour site more efficiently than non-selected MSC. In vitro, oncolytic adenovirus loaded sNSC showed higher efficiency of killing glioblastoma cells compared to non-selected NSC. For both cell types (MSC and NSC) podoplanin has been identified as a critical enhancer of cell migratory properties.

Implications of all the available evidence

The concept presented here identifies cell motility and migration as determinants of stem cell efficacy and suggests the use of highly migratory stem cell subpopulations in cell-based therapies, which can improve stem cell homing to the injury site and consequently enhance and potentially stabilize the therapeutic efficacy of transplanted cells.

1. Introduction

Current stem cell (SC) therapies in regenerative medicine employ a broad range of SC classes comprising adult, foetal, induced pluripotent and embryonic SC. One of the remarkable features of SC is their targeted migration to the disease-affected area driven by inflammation, growth factors and chemokines [1]. However, the majority (if not all) SC candidates render a high degree of variability in their therapeutic properties when tested in the same disease condition (for review see [2]). Within one SC class the cells show different paracrine properties depending on their initial tissue source. For instance, mesenchymal stem cells (MSC) isolated from dental pulp and adipose tissue have distinct expression signatures of genes related to neuronal growth and angiogenesis [3]. Moreover, even within one cell entity from the same tissue source (for instance MSCs from bone marrow [BM] or umbilical cord) the existence of subpopulations with substantial heterogeneity in terms of resistance to stress or self-renewal capacity has been identified in vivo and in vitro [4,5]. The new concept presented herein is based on the premise that besides disease-specific chemotactic and humoral cues guiding SC targeted migration, strong motility and migration capacity of applied SCs are key prerequisites for their sufficient delivery to the desired anatomic locations. Accordingly, we hypothesized the existence of SC subpopulation with high migratory capacity superior to that of other cells within one cell preparation. Identification of such subpopulations would empower cell-based therapies (CBT) with efficacious delivery of SC to the diseased organ irrespective of their administration route and it would provide evidence for the relevance of SC homing for their therapeutic efficacy. As an example, the use of SC for the transport of oncolytic agents in cancer therapies requires their active migration to the tumour site [6]. Poor to non-existent in vivo migration of surgically transplanted neural stem cells (NSC) [7] or MSC [8] reduced the grafted cells ability to reach multiple disease-affected areas of the brain. The requirement not only to migrate, but to do it as fast as possible is of special importance for oncovirolytic cancer therapy. This criterion is dictated by the time gap given for virus-loaded SC to reach the tumour cells until virus-induced cell lysis and death occur [9].

Non-invasive intranasal administration (INA) is gaining increasing attention for its proven delivery and therapeutic efficacy in various preclinical disease models including Parkinson's, Huntington, and Alzheimer's (AD) disease, as well as stroke, multiple sclerosis and neonatal cerebral ischemia [10–15]. However, after INA or intraparenchymal application, SC must traverse considerable distances to reach the desired location, especially when treatment of disease with multifocal pathology is intended. Indeed, the first clinical data suggests a positive correlation between the therapeutic cells' migration potential and long-term clinical outcome [16,17].

Of all cell types, MSC and NSC are the most commonly used in preclinical and clinical trials in oncologic and degenerative diseases of the brain [18–21]. Hence, they were our first choice to test the existence of subpopulations with high migratory properties. This work

aimed to prove that SC migratory capacity determines their homing to disease-affected tissue within the brain as exemplified in in-vivo models of glioblastoma (GBM) and AD. Finally, to justify the importance of this concept for the success of CBT, we compared the functional efficacy of a highly migrating MSC subpopulation and their parental non-selected cell counterparts in slowing down AD-like pathology in vivo.

2. Materials and methods

2.1. Overview of in vitro and in vivo studies

The highly migrating subpopulation of bone marrow MSC (sMSC) was isolated from original murine MSC (oMSC). Both, sMSC and oMSC were characterized by in vitro migration and differentiation assays, flow cytometry analyses of cell surface markers, in vitro migration distance and velocity parameters, population doubling time, cell diameter, small extracellular vesicles (small-EVs) and trophic factor release (NGF, IGF-1, GDNF and VEGF). Transcriptome analysis of sMSC and oMSC identified podoplanin (PDPN) as promising target and flow cytometry confirmed increased PDPN expression on sMSC. To elucidate the role of PDPN in migration of SC, PDPN siRNA silencing was performed with sMSC, while its overexpression by PDPN mRNA transfection was examined with oMSC.

Next, we performed comparative analyses of oNSC and sNSC from a human neural stem cell line (HB1.F3) for their migration capacity, for ability to migrate towards conditioned medium of LNT-229 glioma cells and ability to kill glioma cells.

To characterize the efficacy of SC to slow down the AD-like pathology and to target tumour cells in vivo, murine oMSC and sMSC were applied intranasally in transgenic APP23xPS45 and 3xTg-AD mice, as well as stereotactically injected into the brains of C57BL/6 mice harbouring orthotopic murine glioblastoma. Transgenic AD models were tested for neuronal hyperactivity, memory deficits (by T-maze test) and the brain content of amyloid beta ($A\beta$) peptides and plaques, as well as markers of neurogenesis, synaptogenesis, neuronal survival, inflammatory response (including the quantification of immune cells) and proliferation activity (by BrdU).

In mice harbouring orthotopic GBM, the tumour imaging and tumour volumes were assessed by MRI after oMSC or sMSC injection.

In both, AD and GBM models, oMSC and sMSC were quantified in areas of interest, such as tumour area in the GL-261 glioblastoma model and olfactory bulb (OB), cortex, hippocampus (HC), striatum, cerebellum and brainstem in the 3xTg-AD model.

2.2. Ethics statements

Permission to use the human neural stem cell line (HB1.F3) was granted by the University of British Columbia Clinical Research Screening Committee for Studies Involving Human Subjects. All animal experiments were carried out in accordance with institutional animal welfare guidelines and approved by the local institutional committee of Animal Welfare in Tübingen (Regierungspräsidium Tübingen).

2.3. Primary cells, cell lines and cell cultures

Murine eGFP^{+}BM-MSC were isolated from 6 weeks old male C57BL/6-Tg(UBC-GFP)30Scha/J mice (Jackson Laboratories, Bar Harbor, ME). BM cells were flushed out of the tibiae and femora under sterile conditions, washed with PBS, counted and seeded at a density of 1×10^5 cells per cm^2 in culture medium composed of α-MEM (Lonza, Walkersville, U.S.A.), 1% PS (Lonza) and 10% FCS (Lonza) to tissue culture flasks (Nunc, Roskilde, Denmark). The resulting passage (P) 0 cultures were kept at 37°C in a humidified atmosphere with 5% CO_2. Subconfluent MSC were detached using Trypsin-EDTA, counted and plated to fresh tissue culture flasks for the subsequent passages at a density of 1000 cells per cm^2.

Hippocampal and cortical primary cultures were isolated from neonatal C57BL/6 mice (Charles River Laboratories, Sulzfeld, Germany). Dissected hippocampal and cortical tissue of 6-7 mouse pups (postnatal day 1) were passed through a 100 μm nylon mesh to obtain a single-cell suspension. Both cell cultures were expanded in Neurobasal Medium supplemented with B-27 supplement, 2mM L-Glutamine (Gibco, ThermoFisher, Darmstadt, Germany) and 2% FCS (Biochrom, Millipore, Berlin, Germany) at 37°C in a controlled-atmosphere (5% CO_2).

The human NSC line (HB1.F3) was cultured in DMEM High Glucose (Gibco) supplemented with 10% FCS (Biochrom) and 100 mM sodium pyruvate (Biochrom) at 37°C with 10% CO_2.

2.4. Selection of highly migrating subpopulations from murine BM-MSC

To select and purify the highly migrating murine BM-MSC subpopulation (sMSC), the original murine BM-MSC population (oMSC) was expanded and seeded onto a ThinCert^{TM} 6-well cell culture insert (8×10^5 cells, 8 μm pore size, Greiner Bio-one, Frickenhausen, Germany) and placed over the culture medium containing DMEM high glucose (Gibco) supplemented with 10% FCS and 1mM sodium pyruvate (Biochrom). The highly migrating sMSC subpopulation was harvested from the bottom side of the membrane after 1 hour and sub-cultured for further experiments.

2.5. In vitro MSC differentiation assays

We assessed the differentiation potential of murine oMSC and sMSC into the adipogenic, osteogenic and chondrogenic lineage as described previously [22]. Briefly, for adipogenic and osteogenic differentiation, MSC were seeded at a density of 1,000 cells per cm^2 and kept under standard culture conditions until reaching subconfluency. Subsequently, either adipogenic differentiation was induced using the MSC Adipogenic BulletKit (Lonza), or osteogenic differentiation was induced using "osteogenic medium" composed of α-MEM (Lonza), 1% PS (Lonza), 10% FCS, 10^{-8} M dexamethasone, 0.2 mM ascorbic acid and 10 mM β-glycerolphosphate (Sigma-Aldrich). After three weeks under differentiation conditions, lipid vacuoles in adipogenic cultures were stained with Oil Red O and calcium deposits of osteogenic cultures with Alizarin Red S, respectively. For chondrogenic differentiation, 2.5×10^5 MSC were kept in micromass pellet cultures. Differentiation was induced using the MSC Chondrogenic Differentiation BulletKit (Lonza), supplemented with TGF-β 3 (Lonza) as a growth factor. After four weeks of differentiation, frozen sections of fixed pellets were performed and stained with Alcian blue.

2.6. Flow cytometry analyses

To characterise the surface epitope pattern of murine BM-MSC, flow cytometry analysis of surface marker expression was performed with a FACScan cytometer (BD Biosciences, Heidelberg, Germany) using BD CellQuest Pro^{TM} software. Flow cytometry analyses of murine BM-MSC were performed using the following antibodies: anti-CD9, -CD29, -CD34, -CD39, -CD43, -CD44, -CD105, -CD106, -CD146 and -Sca-1. All antibodies were from BD Biosciences except for anti-CD34 (AbD Serotec), -CD39 (R&D), -CD146 (BioLegend), and -CCR4 (R&D).

To evaluate the expression of PDPN after the *PDPN* mRNA transfection in oMSC-GFP and oHB1.F3, cells were detached and washed with DPBS. Afterwards, the staining of PDPN on oMSC-GFP was performed with PE labelled Syrian hamster anti-mouse PDPN antibody (BioLegend) and on HB1.F3 cells with PE labelled rat anti-human PDPN antibody (BioLegend) for 30 min. Afterwards, the cells were washed twice with DPBS, fixed in 1x CellFix solution (BD

Biosciences), and analysed immediately using the FACScan flow cytometer (BD Biosciences). The gating strategy of PDPN expression is shown in **Supplementary Fig. 6**.

To assess the number of CD11b, CD85, F4/80, MHC II and BrdU positive cells in the brain of 3xTg-AD mice after INA of o/s MSC or vehicle, one hemisphere per mouse was dissociated with a cell strainer (100μm). The cell suspension was centrifuged at 350 x g for 5 min and cells were stained with F4/80-Pacific Blue (1:100), CD11b-APCeFluor780 (1:200), CD86-PE (1:400), and MHC II-PerCP (1:400) (all BD Bioscience) for 20 min at 4°C. The incubated cells were washed with PBS and fluorescence of one half was measured with a FACS-Canto II cytometer (BD Bioscience) and analysed with FLowJo software. The other half of cells was additionally stained with anti-BrdU according to the manufacturer's manual (APC-BrdU Flow Kit, BD).

2.7. Determination of cell viability and diameter

Cellular viability and diameter of detached cells were examined with the CASY®2 Cell Counter and Analyzer System, Model TT (Roche Diagnostics, Mannheim, Germany) according to the ECE method described by Lindl et al. [23].

2.8. In vitro migration assays

To compare the migration potential of murine oMSC and sMSC, both populations (8×10^5 cells) were seeded on a 6-well 8 μm pore ThinCert™ membrane and allowed to migrate over 3 h to the lower compartment containing either cell culture medium only or a culture of adherent neural cells isolated from the hippocampus (HC) or cortex of neonatal mice (3×10^5 cells each). Migrated cells were detached from the bottom side of the membrane with Trypsin-EDTA, allowed to adhere in the 6-well plate for 18 h and quantified by the Cell Titer Blue cell viability assay (CTB, Promega, Mannheim, Germany). The CTB cell viability assay data expressed as fluorescence units were transformed in cell counts using the respective standard curve showing the correlation between the distinct ascending cell numbers and the respective fluorescence units produced by them.

For comparison of non-selected (original) human neural stem cell line (oHB1.F3) with or without *PDPN* transfection, the cells were cultured as described above. For migration assay after *PDPN* transfection with synthetic *PDPN* mRNA in oHB1.F3 NSC, non-transfected oHB1.F3 NSC, oHB1.F3 NSC incubated with transfection medium (TM) only, and PDPN overexpressing oHB1.F3 NSC 72 h after PDPN transfection were seeded on a 24-well ThinCert™ membrane (1×10^5 cells/well) and assessed after 4 h migration by CTB cell viability assay as described for oMSC and sMSC.

2.9. In vitro migration distance and velocity of murine BM-MSC

Cell motility of murine oMSC and sMSC was evaluated by live imaging of cells growing in 6 cm petri dishes. Two hours after seeding (100,000 cells/19.6 cm^2) cells (n=9) were tracked every 30 min. during the period of 20 h with the CellP Soft Imaging System (Soft Imaging System, Münster, Germany). Velocity as well as accumulated and Euclidian distance were determined by manual tracking with the ImageJ plug-in "Manual TrackinG" (http://rsb.info.nih.gov/ij/plugins/manual-tracking.html). Visualization and data analysis of the migration was performed by the Chemotaxis and Migration Tool 2.0 (ibidi GmbH, Martinsried, Germany).

2.10. Quantification of murine oMSC and sMSC population doubling times

To determine their population doubling time murine oMSC or sMSC were seeded in triplicate in 6 cm culture dishes (70,000 cells/dish). After 24 h, 48 h, 72 h and 96 h cells were harvested and counted. The generation time was determined with the 24 h and 48 h values and with the 48 h and 72 h values according to the formula GT = (log 2 x T) / (log Y − log X), where T is the duration of culture, X is the cell count at the beginning, and Y is the cell count at the end of cultivation.

2.11. Extracellular vesicle (EV) isolation and nanoparticle tracking analysis

Supernatants of murine o/sMSC were collected and subjected to differential centrifugation (all steps at 4°C): 10 min at 130 x g to clear supernatants from cell debris, followed by 30 min at 10,000 x g to pellet microvesicles (MVs), and ultracentrifugation for 2 h at 100,000 x g to pellet small extracellular vesicles (small-EVs). The final 100,000 x g pellet was re-suspended in PBS and analysed using the Nanosight LM10 system at 23°C (green laser 532 nm, syringe pump, Nanosight 2.3 software). The following settings were used: Camera level =16, particle detection with a screen gain of 16, a detection threshold of 7 and the setting "minimum expected particle size auto". A script control was used (repeat start, syringe load 500, delay 5, syringe stop, delay 15, capture 30, repeat 4). Per sample five 30 s videos were recorded, the particles were tracked and average values were calculated to express particle number over size.

2.12. *siRNA* podoplanin *silencing*

One day before transfection, murine sMSC were cultured in x-well Tissue Culture Chambers (18,000 cells/chamber, 8-well on lumox, Sarstedt, Nuembrecht, Germany). Transfection medium alone or 50 pmol siRNA duplex (Santa Cruz Biotechnology, Inc., Heidelberg, Germany) were added to the serum-free culture and incubated for 18 h. Transfection was stopped by adding the equal volume of DMEM supplemented with 20% FCS and the cells were incubated for additional 24 h. The medium was then aspirated and replaced with DMEM containing 10% FCS. After 24 h and 11 days the siRNA transfection was repeated under the same conditions.

The efficiency of *PDPN* siRNA silencing was tested with the migration assay using 60,000 cells on a ThinCert™24-well plate (8 μm pore size). Cultures of sMSC supplemented with DMEM or TM as controls were assayed for 3 h against siRNA transfected cells. Quantification of migrated cells was performed with the CTB assay (Promega).

2.13. Podoplanin *mRNA transfection*

The pEX-A2 plasmid containing the coding sequence (CDS) of murine or human *PDPN* was obtained from Eurofins Genomics (Ebersberg, Germany). Synthetic *PDPN* mRNA was generated as previously described [24]. Briefly, the plasmid insert was amplified by polymerase chain reaction (PCR) and a poly T120-tail was added. Subsequently, mRNA was synthetized from the PCR product using the MEGAscript T7 Kit (Life Technologies). The *in vitro* transcription (IVT) was performed for 4 h at 37°C and 40 μl IVT mixture contained 1 μg PCR product, 2.5 mM 3′-O-Me-m7G(5′)ppp(5′)G RNA cap structure analogue (New England Biolabs, Frankfurt am Main, Germany), 7.5 mM ATP, 1.875 mM GTP (both from MEGAscript® T7 Kit), 7.5 mM Me-CTP, 7.5 mM Pseudo-UTP (both from TriLink BioTechnologies, San Diego, U.S.A.), 40 U RiboLock RNase inhibitor (ThermoFisher Scientific, Waltham, MA, U.S.A.), 1 × reaction buffer, and 1 × T7 RNA polymerase enzyme mix. After IVT, 1 μl TURBO DNase (from MEGAscript® T7 Kit) was added to the reaction mixture and incubated for 15 min at 37°C to remove the template DNA. Synthesized mRNA was purified using RNeasy Mini Kit (Qiagen, Hilden, Germany) according to manufacturer's instructions. Afterwards, the mRNA was treated for 30 min at 37°C with Antarctic phosphatase (5 U/μl) (New England Biolabs) to remove 5′ triphosphates. The treated mRNA was purified

using RNeasy Mini Kit according to manufacturer's instructions. The concentration was measured using ScanDrop spectrophotometer (Analytic Jena, Jena, Germany). The quality and purity of synthesized modified mRNA was determined by 1% agarose gel electrophoresis. The mRNA was stored at -80°C and used for transfections.

To perform *PDPN* mRNA transfections, 150,000 oMSC or 300,000 HB1.F3 cells were seeded per well of a 6-well plate and incubated overnight at 37°C in a CO_2-incubator. The next day, the mRNA transfection of cells was performed. To form the transfection complexes, 1.5 μg *PDPN* mRNA was added to 1 mL Opti MEM I containing 3 μL Lipofectamine 2000 (Life Technologies) and was incubated for 20 min at room temperature. Cells were washed with 1 mL DPBS and then incubated for 4 h at 37°C with transfection complexes. Subsequently, the complexes were replaced by culture medium. The expression of PDPN was measured using flow cytometry 24 h (oMSC) and 72 h (HB1.F3 cells) after transfection.

2.14. Immunohistochemistry

For the analyses of APP/Aβ, DCX, NeuN, TUNEL, and murine eGFP-oMSC/sMSC, 20μm thick sagittal brain sections of APP23xPS45 and 3xTg-AD mice were fixed in 4% paraformaldehyde for 15 min and washed with PBS. The samples were incubated with antibodies against APP/Aβ (rabbit polyclonal, dilution 1:100, Sigma-Aldrich, St. Louis, MO, U.S.A. or mouse monoclonal 6E10 antibody (dilution 1:1000, BioLegend, San Diego, CA, U.S.A.), doublecortin (DCX, polyclonal, dilution 1:1000, Abcam, Cambridge U.K.), NeuN (rabbit polyclonal, 1:500, Abcam, Cambridge, U.K.) and eGFP (rabbit polyclonal, 1:1,000, Novus Biologicals). For immunofluorescence detection samples were stained with goat anti-mouse Cy3 (1:800; Jackson Immuno Research Laboratories, Inc. West Grove, U.S.A.), goat anti-rabbit FITC (1:200; Jackson Immuno Research Laboratories, Inc. West Grove, U.S.A.), or goat anti-rabbit DyLight 405 (1:500; ThermoFisher Scientific). For BrdU tracking the subgroups of vehicle or o/sMSC treated 3xTg-AD (n=3 in each) mice were orally fed on the last 3 days prior to sacrificing with BrdU (1mg/mL in drinking water) and additionally were intraperitoneally injected with BrdU (2mg in 200μL PBS). For BrdU post-mortem staining, a Cy3 conjugated rabbit anti-BrdU polyclonal antibody (1:500, Bioss) was applied.

For quantification of NeuN/TUNEL positive cells in 3xTg-AD mouse brain, sections pre-stained with anti-NeuN antibodies were further processed for TUNEL labelling with In Situ Cell Death Detection kit TMR red (Sigma-Aldrich) according to the manufacturer's protocol.

Samples were embedded in mounting medium containing 4′,6-diamidino-2-phenylindole (DAPI) for nuclear staining and documented with a fluorescence microscope (Olympus Optical Co. Europe, Hamburg, Germany) and Analysis DOKU® software (Soft Imaging System GmbH, Leinfelden-Echterdingen, Germany).

2.15. Human HB1.F3 neural stem cell line migration and adenoviral infection

HB1.F3 cells were transfected as described above. The cells were harvested 24 h after transfection, counted and each 800,000 cells in suspension were infected with 200 MOI of the oncolytic Ad-Delo3-RGD [9] or were left untreated. 2 h after infection, these cells were applied into the upper part of 6-well transwell migration chambers (8 μm pores, Greiner Bio-One) and were allowed to migrate towards conditioned medium of LNT-229 glioma cells for 4 h. To analyse tumour cell killing capacities migrated human NSC were harvested using Accutase™ (Sigma-Aldrich), counted and added to 100,000 stably eGFP-transfected LNT-229 glioma cells [25] growing in 6-well plates. Images of cells in culture were taken every day with a Zeiss fluorescent microscope using the Axiovision software (Zeiss). Glioma cell growth and oncolysis were quantified by measuring the area covered by LNT-229 ^{GFP} cells using the IMAGE J software (NIH, U.S.A.).

2.16. RNA isolation and qRT-PCR analyses

Brain homogenates of 13-months old 3xTg-AD mice were lysed with RLT-Buffer and for RNA isolation the RNA Mini Kit (Qiagen) was applied according to the manual. Reverse transcription of RNA was performed with the Transcriptor High Fidelity cDNA Synthesis Kit (Roche) according to the protocol provided. For quantitative PCR 50 ng cDNA were used.

Quantitative PCRs were performed with a LightCycler 480 (Roche) with a primary 5 min denaturation step at 95°C; 45 cycles with 10 sec of denaturation at 95°C, 10 sec annealing at 60°C and 10 s elongation at 72°C; and a melting curve as a final step with 5 s at 95°C and 1 min at 65°C. The PCR products were stored at 4°C until analysis on a Qiaxcel (Qiagen).

Primers for IL-6 were sense (5'-TGATGGATGCTACCAAACTGG-3') and antisense (5'- TTCATGTACTCCAGGTAGCTATGG-3') and generated a product of 96 bp. Primers for IL-10 were sense (5'-CAGAGCCACATGCTCCTAGA-3') and antisense (5'-TGTCCAGCTGGTCCTTTGTT-3') and generated a product of 79 bp. Primers for neprilysin were sense (5'-GGGAGGCTTTATGGAAGC-3') and antisense (5'- CCGGATTTGTGCAATCAAGT-3') and generated a product of 75 bp. Primers for PSD95 were sense (5'-GACGCCAGCGACGAAGAG-3') and antisense (5'-CTCGACCCGCCGTTTG-3') and generated a product of 96 bp.

PCR results were analysed by normalizing the expression of each target gene to the expression of the housekeeping gene β-actin in each sample. Primers for β-actin were sense (5'-AAGGCCAACCGTGAAAAGAT-3') and antisense (5'-GTGGTACGACCAGAGGCATAC-3') and generated a product of 110 bp.

2.17. Microarray based transcriptome analysis

High quality total RNA was isolated from murine oMSC and sMSC from three consecutive passages each using the mirVana™ miRNA Isolation Kit (ThermoFisher Scientific). RNA quality was assessed through determination of RNA integrity number (RIN) using Agilent Bioanalyzer (Agilent Technologies). Subsequently, RNA samples from three oMSC and sMSC passages were analysed using Affymetrix GeneChip Mouse Gene ST 2.0 arrays (Affymetrix, Santa Clara, CA, U.S.A.) according to the manufacturer`s protocol.

For the six arrays, quality control and pre-processing using Robust Multi-array Average [26] was performed with Affymetrix Expression Console (Build 1.3.1.187). Based on the pre-processed log2 signal intensities, a two-tailed paired t-test comparing sMSC and oMSC samples paired by cell culture passage was computed using statistical software R-3.0.2 [27]. A probe set was considered as being relevantly altered between the paired sMSC and oMSC samples, if the median of the three log2 fold changes was greater than 1 in absolute value and if the median log2 signal intensity in oMSC and/or sMSC was greater than 6. Here, the latter condition ensures sufficient expression levels in at least two passages of at least one group. Heatmaps displaying the log2 signal intensities were generated by R-3.0.2.

The complete microarray data set has been deposited at the European Genome-phenome Archive (EGA), which is hosted by the EBI and the CRG, under accession number EGAS00001002478. Further information about EGA can be found on https://ega-archive.organd "The European Genome-phenome Archive of human data consented for biomedical research" [28].

2.18. Protein isolation and Western blot analyses

Western blotting was performed using protein lysates from brain homogenates of 3xTg-AD mice. The total protein was determined by DC Protein assay (Bio-Rad). For each lane, 50 μg of protein were

subjected to sodium dodecyl sulfate polyacrylamide gel electrophoresis in a 12.5% or 10% gel and transferred to PVDF membranes by tank blotting. Membranes were blocked in 0.66 % (v/w) I-Block or 5% w/v nonfat dry milk (both from Tropix, Applied Biosystems, Weiterstadt, Germany) in PBST or TBST (0.05% Tween 20 in PBS or TBS, with and pH 7.4) for 1.5 h. Antibodies against synapsin (1:1000, Cell Signaling, Cambridge, United Kingdom), synaptophysin (1:1000, Cell Signaling), ionized calcium binding adaptor molecule 1, Iba-1 (1:1000, Wako, Neuss, Germany), ChAT (1:1000, Millipore), and GAPDH (1:1000, loading control, Millipore) were used.

To confirm the efficacy of *PDPN* siRNA silencing in sMSC 50 μg protein from cell lysates per lane was subjected to a 10-20% Tris-Tricine-Gel (Invitrogen, ThermoFisher) and transferred to a 0.45 μm Immobilon-P membrane (Merck Millipore) by tank blotting. The membrane was blocked with 0.66% I-Block (Tropix, Applied Biosystems, Weiterstadt, Germany) in TBST for 1 h, followed by incubation at 4°C overnight with rat anti-PDPN (1:1000, LSBio, Biozol).

For visualization of antibody binding, membranes were incubated with alkaline phosphatase- or Cy2/Cy5-conjugated antibodies for 2 h at RT. Protein bands were visualized using chemiluminescence or fluorescence detection systems (Bio-Rad, Hercules, CA). For imaging and densitometric analyses a VersaDocTM 4000 MP imaging system (Bio-Rad) was used. Data were normalized to the respective densitometric values of loading controls (GAPDH).

2.19. ELISA, Luminex® and V-plex® assays

Brains of 13-months old 3xTg-AD mice after INA of murine oMSC and sMSC were homogenized in ice cold PBS containing Protease Inhibitor Cocktail Tablets (Roche, Sigma-Aldrich). Homogenates were clarified by centrifugation for 10 min at 16,000 x g, the supernatant was aliquoted and frozen at -80°C. Quantitation of protein content was done by using the BIO-Rad DC Protein Assay (Bio-Rad) according to the manufacturer's manual.

Cell culture supernatants of murine oMSC and sMSC were collected 48 h after plating the cells. Both, brain homogenates and cell culture supernatants were analysed with a GDNF, IGF-1, NGF and VEGF ELISA (myBiosource, Biozol) according to the manufacturer protocols. The data are normalized to pg growth factor/mg protein from the tissue or cell lysates from which the cell culture supernatants were collected.

Aβ 40 and 42 in brain homogenates or cell culture supernatants were quantified using the Aβ 40 and 42 Brain Elisa Kit or High Sensitivity Elisa Kit respectively (Millipore, Darmstadt, Germany). Therefore, reagent blank, standards (range 16 pg/mL - 500 pg/mL), controls and samples were measured according to the manufacturer's manual. Obtained absorbances of the standards were plotted against their concentrations and unknowns are determined with a linear regression model. The results are presented as pg Aβ /mg total protein.

The brain levels of TNFα, IL-12, IL-6 and IL-10 in 3xTg-AD mice were measured using the V-plex® Cytokine Mouse customized panel (Mesoscale Discovery, Rockville, MD, U.S.A.) according to the manufacturer's instructions. The data were acquired on a Mesoscale Discovery Sector Imager 6000 and analysed using the Discovery Workbench 3.0 software (MSD). The results are presented as pg/mg total protein.

2.20. Transgenic Alzheimer's mice and intranasal delivery of murine BM-MSC

For delivery of murine eGFP$^+$ o/sMSC in Alzheimer's transgenic mice, 6-7-month old APP23xPS45 animals of either sex (C57Bl/6-Tg (Thy1-APP*Sw,Thy1-PS1*G384A)1Sdz) originally supplied by M. Staufenbiel (Novartis) and 6-month old female *vs.* 13-month old male 3xTg-AD mice (B6.129-Psen1tm1Mpm Tg(APPSwe,tauP301L) 1Lfa/ Mmjax) obtained from Jackson Laboratory (Bar Harbor, strain provider: Frank LaFerla, University of California Irvine, CA, U.S.A.) were used. Intranasal cell or vehicle (PBS) application was performed on awake animals. All animals received twice for each nostril alternate applications (left-right) of 6 μL drops containing 100 U hyaluronidase (Sigma-Aldrich) dissolved in 24 μl sterile PBS. Cell suspension (1×10^6 MSC in 40 μL of sterile PBS) or vehicle (PBS) was applied thirty minutes after intranasal pre-treatment with hyaluronidase following the same procedure, i.e. in alternating 10 μL portions for each nostril. Cell and vehicle administration were repeated on day 3 after the first INA. Three weeks after INA the animals (3xTg-AD mice) were either euthanized under CO_2 or further processed for the measurement of in vivo neuronal hyperactivity (APP23xPS45 mice) described below. On the last 3 days prior to sacrificing, 13-months old 3xTg-AD mice (n= 3 in each group) treated either with oMSC/sMSC or vehicle received BrdU as described above. The brains of euthanized mice were stored at -80°C until further histochemical, PCR, ELISA and V-PLEX analyses.

2.21. Murine orthotopic brain tumour models and murine BM-MSC implantation

Mouse glioblastoma GL-261-Luc (PerkinElmer LAS GmbH, Rodgau-Juegesheim, Germany) cells were stereotactically implanted (1×10^5 cells in 2μL of sterile PBS) into the brain (coordinates relative to bregma: DV -3.0; AP +1.0; ML -1.5) of 8-weeks old male C57BL/6 mice (Charles River Laboratories). At day 15 after tumour cells implantation 1×10^5 eGFP+ murine oMSC vs. eGFP+ sMSC (n=7 per group) were injected contralaterally to the position described above. All injections were performed with a 26 gauge needle (Hamilton, Bonaduz, Switzerland). Total injection volume was 2 μL at a flow rate of 1 μL/min. A mixture of 0.5 mg/kg medetomidin, 5.0 mg/kg midazolam and 0.05 mg/kg fentanyl was used for anaesthesia, which was abrogated with 0.5 mg/kg flumazenil and 2.5 mg/kg atipamezole. Animals were euthanized under CO_2 at day 7 after injection of murine oMSC/sMSC.

2.22. MR imaging

One day before and 6 days after implantation of MSCs MR scans were performed. Therefore, a mixture of 1.5% isoflurane (Abbott, Wiesbaden, Germany) evaporated in oxygen at a flow of 0.5 L/min was used to anesthetize the animals. Mice were placed in a 7T ClinScan MR-Scanner (Bruker, Ettlingen, Germany) and T2-weighted images of the brain were acquired with a dedicated brain coil. A heating system connected to a rectal temperature sensor maintained the body temperature at 37 °C. Inveon Research Workplace 3.1 (Siemens Preclinical Solutions, Erlangen, Germany) was used for image analysis.

2.23. T-maze test

Spatial memory of 6-months and 13-months old 3xTg-AD mice was assessed by T-maze forced choice alternation after 4-days habituation period, in which the mice were allowed to explore the T-maze apparatus for 5 minutes per day or until the reward (sucrose pellet) placed in the goal arm was found and consumed. In 16-days assessment period the training consisted of 6 paired ("sample" and "choice") trials per day. In the "sample" trial, one of the goal arms was closed and the mouse was forced to select the opposite arm. The order of the open goal arms in the "sample" trial was counterbalanced. After 20 s of consuming the reward, the mouse was returned to the start box. On the choice trial, both goal arms were accessible. The mouse was rewarded only for selecting the previously unvisited arm. The paired trial was repeated 6 times with a 15 s interval between each paired trial. The entire period of testing was divided into 4 blocks with 4 consecutive days of testing in each. The test

started on day 1 (10 days prior to INA of MSC *vs.* vehicle). The test block 1 shows the performance of all animals assigned into the treatment groups prior to the INA. The test was continued 10 days after intranasal delivery of either cells of the vehicle until day 26 (test blocks 2-4) after which the animals were euthanized under CO_2. The percentages of correct choices out of total 6 "choice" trials on each of tested days were included into the results of the respective test block, while the latencies (in seconds) to reach the correct arm were assessed on the last day of each test block.

2.24. Assessment of neuronal hyperactivity by in vivo Ca^{2+} imaging of layer 2/3 cortical neurons

APP23xPS45 mice (7-8 months old) were used to measure spontaneous Ca^{2+} oscillations in cortical neurons. Preparation was essentially performed as described before [29,30]. Briefly, mice were anesthetized using isoflurane in pure oxygen (2.5% for induction; 1-1.5% during surgery) and placed on a warming plate. After skin removal, a custom-made recording chamber was glued to the skull. Afterwards, the bone covering the cortical region of interest was thinned using a dental drill. The mouse was positioned on a warming-plate under the microscope, supplied by 0.8-1.5% isoflurane, and the perfusion chamber was continuously perfused with pre-warmed extracellular perfusion saline containing (in mM): 125 NaCl, 4.5 KCl, 26 $NaHCO_3$, 1.25 NaH_2PO_4, 2 $CaCl_2$, 1 $MgCl_2$, 20 glucose, pH 7.4, when bubbled with 95% O_2 and 5% CO_2. A small craniotomy was placed over the frontal cortex using a thin injection needle. The neurons were stained with the fluorescent Ca^{2+} indicator dye Oregon Green BAPTA-1 (OGB-1) using multi-cell bolus loading following the protocol described before [30].

Time-lapse imaging of layer 2/3 cortical neurons was performed with a custom-built two-photon laser scanning microscope based on a mode-locked laser operating at 690-1040 nm wavelength (MaiTai, Spectra Physics, Mountain View, CA, U.S.A.) and a laser-scanning system (Olympus Fluoview, Olympus, Tokyo, Japan) coupled to an upright microscope (BX51WI, Olympus Tokyo, Japan). All images were collected at a frame rate of 7-8 Hz. Spontaneous Ca^{2+} activity of neurons was recorded over a time period of approximately 6 min.

Frequency distribution of spontaneous Ca^{2+} transients in the recorded neuronal population was compared using the Kolmogorov-Smirnov-test. Distributions of the fractions of silent, normal and hyperactive cells were compared using Chi-square test.

2.25. Statistical analyses

All data are given as means ± standard deviation (SD) or standard error of means (SEM). For multiple comparisons in in vitro and in vivo experiments (Fig. 1a,b; Fig. 2a; Fig. 3a,b; Fig. 4a,c; Fig. 5b,c; Fig. 6a,b,c,e; Fig. 7a,b; Suppl.Fig.1d; Suppl. Fig.3-5), one-way analysis of variance (ANOVA) followed by Bonferroni's post-hoc test was

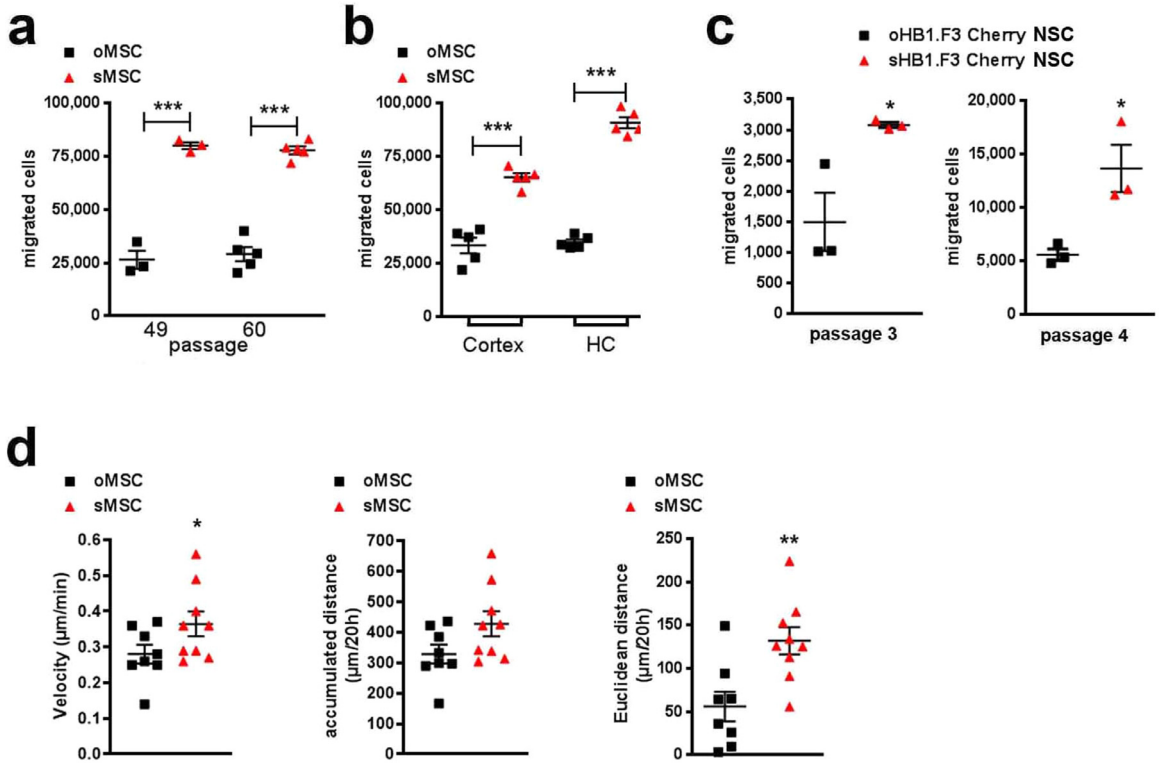

Fig. 1. In vitro migration potential, characterization and function of murine MSC and human NSC subpopulations

(**a**) Migration capacity of oMSC and sMSC over 3 h at two passages (P49 and P60), *n*=3-6, each data point represents one biological replicate per group; exemplary experiment of 8 independent experiments; cell numbers of migrated oMSC vs. sMSC in two different passages were compared with ANOVA and Bonferroni's multiple comparisons test (***p <0.001). Error bars: SEM.

(**b**) Migration of oMSC and sMSC over 3 h towards murine cortical (cortex) and hippocampal (HC) primary cultures seeded on the bottom of transwell chambers, *n*=5, each data point represents one biological replicate per group; cell numbers of oMSC vs. sMSC migrated towards cortical and hippocampal cultures were compared with ANOVA and Bonferroni's multiple comparisons test (***p <0.001). Error bars: SEM.

(**c**) Migration over 4.5 h of human o/sHB1.F3 Cherry NSC in passage 3 and 4. The number of floating cells in the lower compartment of the migration chamber was counted after crystal violet staining. Cumulative cell number calculated from 79 optical fields within a 24-well plate, *n*=3 per passage, each data point represents one biological replicate per group out of a single experiment. Cell numbers of migrated oNSC vs. sNSC were compared with two-tailed t-test (*p<0.05); Error bars: SEM.

(**d**) Two hours after seeding (100,000 cells/19.6 cm^2), oMSC and sMSC were tracked every 30 min during 20 h. Velocity, accumulated and Euclidian distance for representative *n*=9 cells were determined by manual tracking. Each data point represents a single cell analysed per group. Two-tailed t-test was used to compare the velocity, accumulated and Euclidian distance of oMSC vs. sMSC (*p<0.05; **p<0.01); Error bars: SEM.

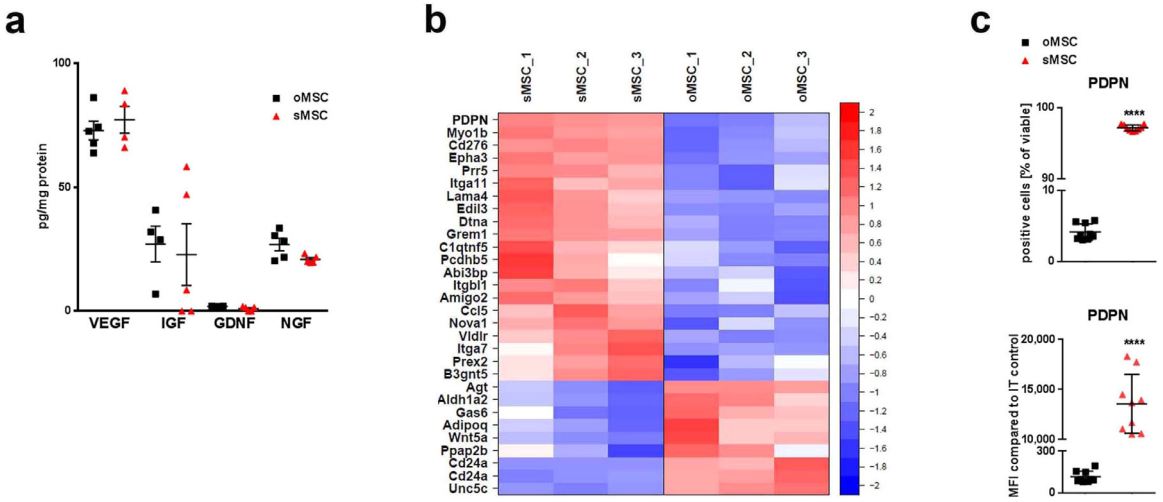

Fig. 2. In vitro paracrine properties and transcriptomic signature of oMSC and sMSC

(**a**) Secreted trophic factors (mRNA clustered in Supplementary Fig.2a) in cell culture supernatants of oMSC and sMSC 48 h after plating of cells analysed by ELISA, *n*=5, each data point represents one biological replicate per group; replicates analysed collectively by specific ELISAs for GDNF, IGF, NGF and VEGF; oMSC were compared with sMSC by ANOVA with Bonferroni's multiple comparisons test. Error bars: SEM; GDNF, Glial cell-derived neurotrophic factor; IGF, Insulin-like growth factor; NGF, Nerve growth factor; VEGF, vascular endothelial growth factor.

(**b**) Heatmap of microarray data displaying genes related to cell migration and/or adhesion. Only genes differing significantly and relevantly between murine oMSC and sMSC are displayed. Row-wise z-scores of normalized log2 signal intensities in murine oMSC and sMSC, *n*=3 per group (3 different passages). Z-scores color-coded as indicated by colour bar on the right.

(**c**) Quantification of PDPN protein by flow cytometry analysis of o/sMSC to validate *PDPN* mRNA expression (microarray), *n*=9, each data point represents one biological replicate per group; two-tailed t-test was used for comparison of percentage and MFI counts of oMSC vs. sMSC (***$p<0.001$); Error bars: SD. IT, isotype control; MFI, mean fluorescence intensity.

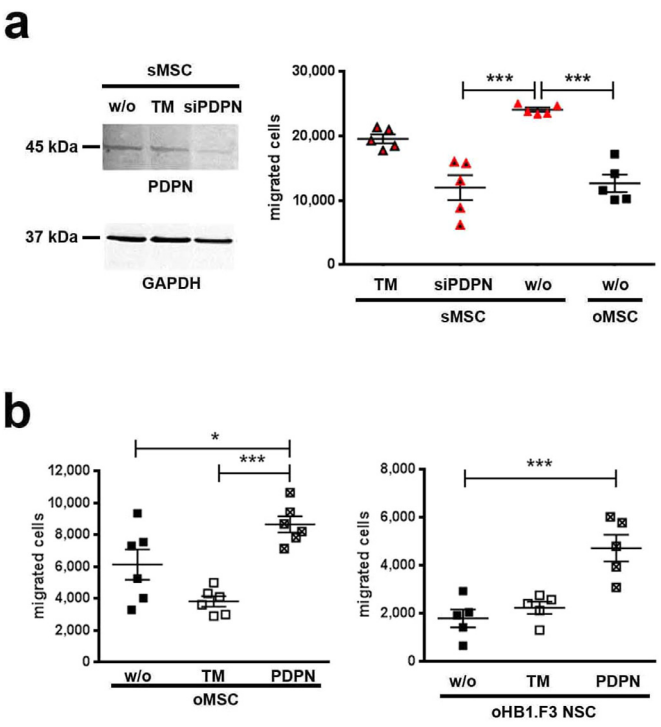

Fig. 3. In vitro loss and gain of PDPN function in MSC and NSC.

(**a**) *PDPN* expression in sMSC was suppressed by siRNA (siPDPN). Shown by Western Blot. Migration was analysed for untransfected (w/o) sMSC, sMSC incubated with transfection medium (TM) only, siPDPN transfected sMSC, and non-transfected (w/o) oMSC (migration time: 3 h), *n*=5, each data point represents one biological replicate per group out of a single experiment; ANOVA and Bonferroni's multiple comparisons test was used to compare non-transfected (w/o) oMSC with siPDPN transfected or untransfected sMSC, (***$p<0.001$). Error bars: SEM.

(**b**) Migration over 4 h of untransfected (w/o) oMSC/oNSC, oMSC/oNSC incubated with TM only, and *PDPN* overexpressing oMSC/oNSC was analysed after 120 h (oMSC) or 72 h (oNSC) after *PDPN* transfection, *n*=6 (oMSC), *n*=5 (oNSC), each data point represents one biological replicate per group; ANOVA and Bonferroni's multiple comparisons test was used to compare PDPN transfected cells with TM-treated or untransfected (w/o) oMSC/oNSC (*$p<0.05$; ***$p<0.001$). Error bars: SEM.

used. Chi-square and Kolmogorov-Smirnov tests were applied to compare relative fractions of cortical neurons and frequency distribution of Ca^{2+} transients in assessment of cortical neuronal hyperactivity (Fig. 6d). For comparison of two groups in all other data sets t-test was employed. All statistical tests were two-tailed and statistical significance level was defined as 5%. Statistically significant results are listed in figure legends.

3. Results

3.1. In vitro migration and podoplanin expression are denominators for highly migrating SC subpopulations

From human NSC and murine MSC original populations (oNSC, oMSC), we selected subpopulations of highly migrating stem cells (sNSC and sMSC) by their fast migration capacity in a transwell migration chamber assay. The subpopulations conserved their superior migration potential towards basal medium or cortical and hippocampal primary cultures over multiple passages (**Fig. 1a-c**) with accordingly increased velocity and migrated Euclidean distance (**Fig. 1d**). Notably, trophic factor secretion (**Fig. 2a**), cell size, EV release, and in vitro differentiation potential (**Supplementary Fig. 1a-c**) were similar between the subpopulations and original populations. sMSC featured greater proliferation potential (**Supplementary Fig. 1d**), and increased expression of CD9, CD44 (H-CAM), CD146 (MCAM) and Sca-1, and decreased expression of CD29 (integrin β1), CD39, CD43, CD105 (endoglin), and CD106 (VCAM-1) (**Supplementary Fig. 1e**).

Furthermore, 30 of 40 genes involved in cell migration and/or adhesion differed significantly and relevantly between sMSC and oMSC (**Fig. 2b**). In contrast, most of the genes related to trophic factors and to the Kyoto Encyclopedia of Genes and Genomes (KEGG) pathways involved in SC aging or cell cycle and proliferation were comparable between the two populations (**Supplementary Fig. 2a, b**). Within the genes involved in migration/adhesion, the top candidate with a 16-fold expression increase in sMSC was podoplanin (*PDPN*), a transmembrane glycoprotein which was confirmed by

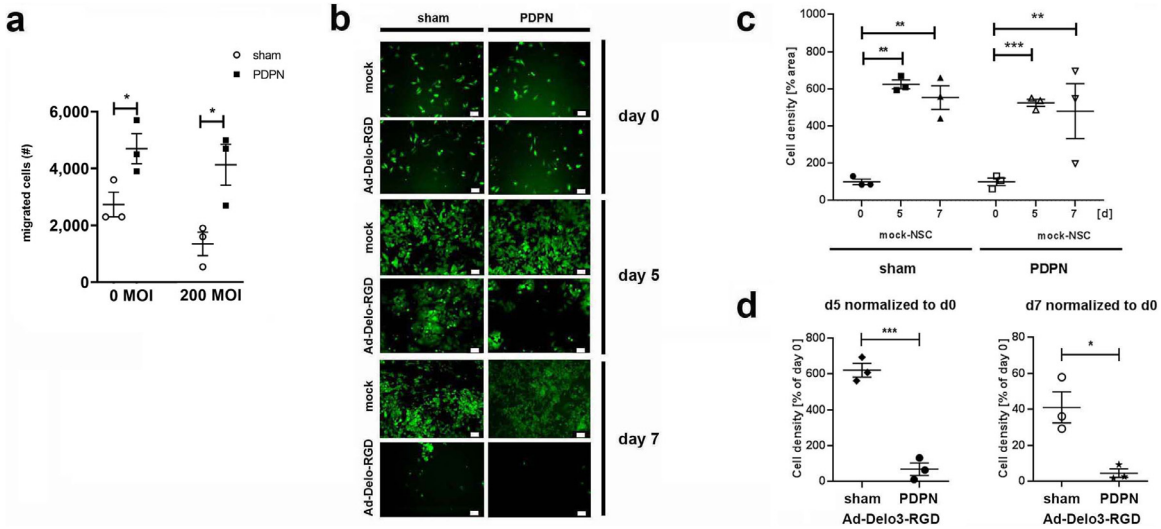

Fig. 4. In vitro glioma tropism and oncovirolytic properties of selected and non-selected human NSC

(**a**) oHB1.F3 NSC transfected with *PDPN* or treated with transfection reagent (sham) were subsequently infected with 200 MOI of Ad-Delo3-RGD to induce oncovirolysis of glioma cells or left untreated (0 MOI; mock) for 2 h, followed by a 4 h migration period through 8 μm transwell membranes towards the conditioned medium from LNT-229 glioma cells. Migrated cells were harvested and counted. Number of migrated mock- or Ad-Delo3-RGD infected F3 NSC after 4h of migration was compared between PDPN-transfected vs. untransfected cells by two-tailed t-test ($^*p<0.05$), n=3, each data point represents one biological replicate per group; MOI, multiplicity of infection; Error bars: SEM.

(b) Migrated NSC with and without PDPN overexpression were co-cultured with eGFP-labelled LNT-229 glioma cells. Representative microphotographs from co-cultures taken at the start (day 0), at day 5 and at day 7 of co-culture. Scale bars: 60 μm.

(**c**) Growth of glioma cells in presence of migrated mock-NSC was quantified as described in methods. Cell density of glioma cells (normalized to the cell density at day 0) in the presence of mock-NSC with and without PDPN transfection was analysed by ANOVA and Bonferroni's multiple comparisons test ($^*p<0.05$), n=3, each data point represents one biological replicate per group out of a single experiment; Error bars: SEM.

(**d**) Growth of glioma cells in the presence of migrated Ad-Delo3-RGD infected F3 NSC. Cell density of glioma cells at day 5 and day 7 is normalized to that of day 0. For comparison of sham- vs. PDPN-transfected NSC two-tailed t-test ($^*p<0.05$) was used, n=3, each data point represents one biological replicate per group; MOI, multiplicity of infection; Error bars: SEM.

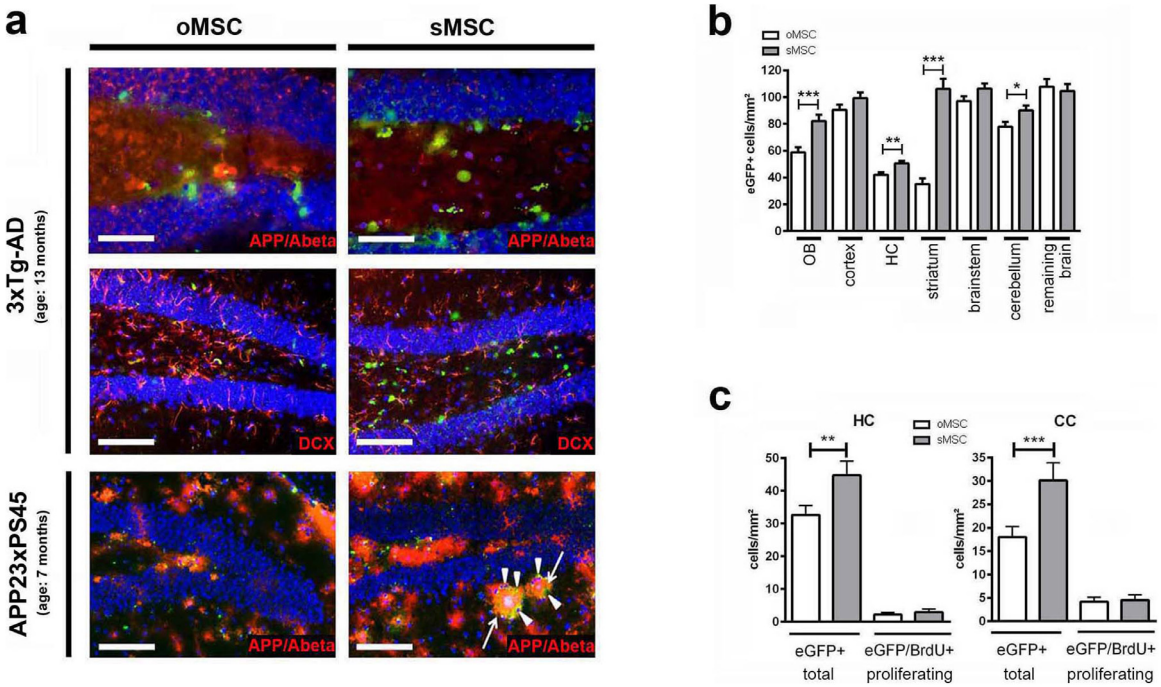

Fig. 5. Localisation and quantification of o/sMSC in the brain of AD mouse models

(**a**) Appearance of eGFP+ oMSC and sMSC (green) in the dentate gyri of 13-month-old 3xTg-AD mice (two upper panels) and 7-month-old APP23xPS45 mice (lower panel). Both animal models show strong expression of APP/Amyloid beta (red). eGFP+ oMSC and sMSC detected in vicinity to DCX positive neurons (red) and circumvent (arrowheads) Aβ plaques (arrows). Scale bars: 100 μm, except for the two microphotographs on the top (50 μm). INA, intranasal application; DCX, doublecortin.

(**b**) Quantification of eGFP+ oMSC and sMSC in different brain regions of 7-month-old 3xTg-AD mice (n=6 per group) after intranasal application (INA) of eGFP+ o/sMSC (2 x application of 1×10^6 cells). 20 sections from each mouse brain were analysed. oMSC and sMSC cell counts normalized to mm^2 were compared in each brain region by two-tailed t-test ($^*p<0.05$; $^{**}p<0.01$; $^{***}p<0.001$). Each column represents ≥60 data points obtained from 20 sections (3-10 micrographs per section); Error bars: SEM. HC, hippocampus; OB, olfactory bulb.

(**c**) Quantification of total eGFP+ o/sMSC and proliferating eGFP/BrdU+ o/sMSC in the HC and CC of 13-month-old 3xTg-AD mice (n=4 per group) after INA. Total o/sMSC were quantified (total oMSC vs. total sMSC) and also compared for their positivity for BrdU (eGFP/BrdU+ oMSC vs. sMSC) from 25 brain sections from each animal by ANOVA and Bonferroni's multiple comparisons test ($^{**}p<0.01$; $^{***}p<0.001$). Each column represents ≥25 data points obtained from 25 sections (1-2 micrographs per section). Error bars: SEM. CC, corpus callosum; HC, hippocampus. (For interpretation of the references to color in this figure legend, the reader is referred to the web version of this article.)

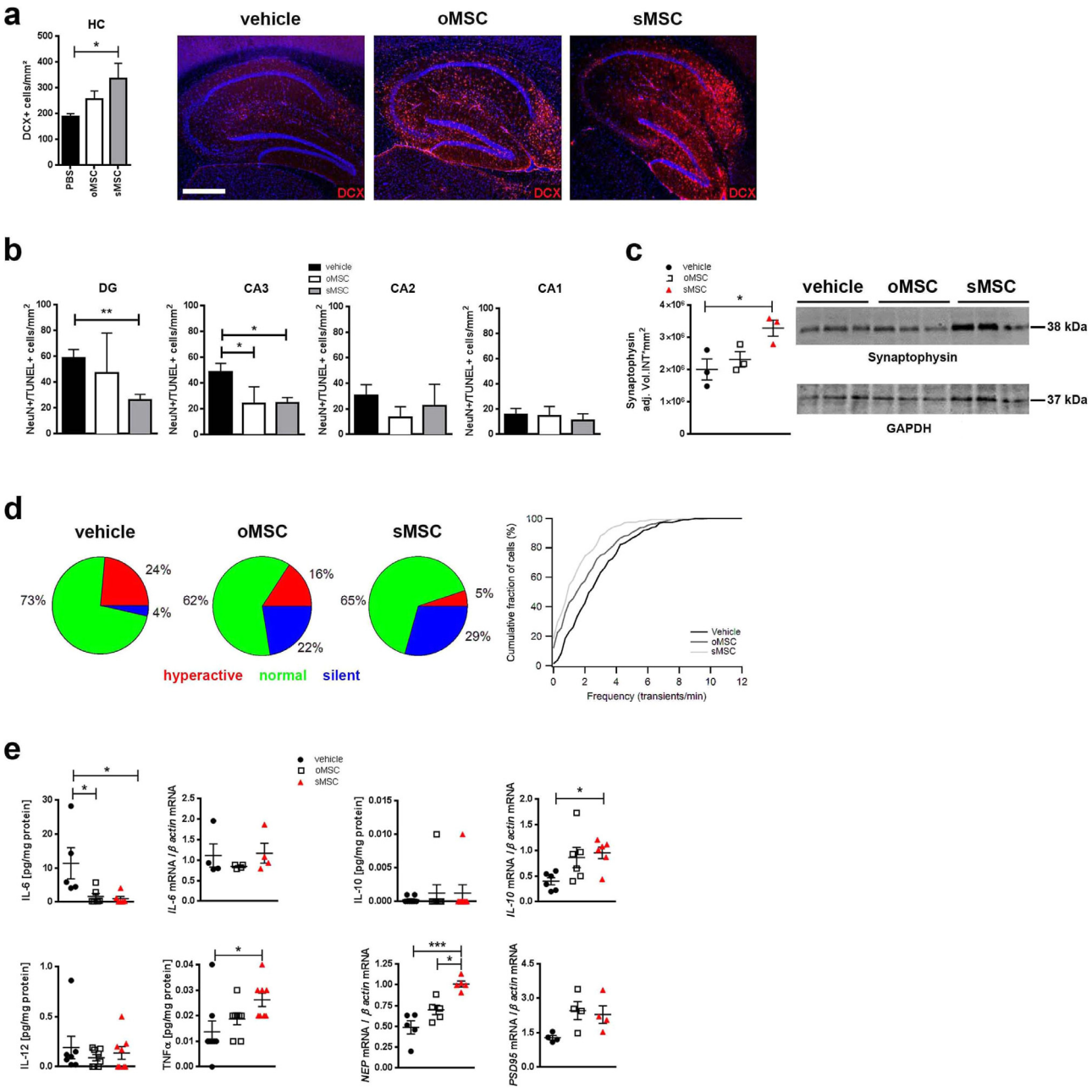

Fig. 6. Neuroprotective and neurogenesis inducing features of oMSC and sMSC in transgenic AD mice

(**a**) Photomicrographs of DCX expression and quantification of DCX+ neurons in the hippocampi of 13-month-old 3xTg-AD mice after INA of o/sMSC (2 x application of 1×10^6 cells, n=3 per group). The number of DCX+ cells was quantified from 10 brain sections of each animal and normalized to mm^2. Each column represents 9-10 data points obtained from 10 sections. ANOVA with Bonferroni's multiple comparisons test was used to compare vehicle-, oMSC and sMSC-treated groups (*p <0.05). Error bars: SEM. Scale bar: 500 μm. DCX, doublecortin.

(**b**) Quantification of NeuN/TUNEL+ neurons in the DG and CA1-3 in 13-month-old 3xTg-AD mice (n=4 per group) after INA of oMSC and sMSC. Cells were quantified in 10 sections from each brain and normalized to mm^2. Each column represents 6-11 data points obtained from 10 sections. ANOVA with Bonferroni's multiple comparisons test was used to compare vehicle-, oMSC and sMSC-treated groups (*p <0.05; **p <0.01). Error bars: SEM. CA, cornu ammonis; DG, dentate gyrus.

(**c**) Western blot with densitometric analysis of synaptophysin in brain homogenates of 13-month-old 3xTg-AD mice (n=3 per group) after INA of oMSC and sMSC. ANOVA with Bonferroni's multiple comparisons test was used to compare vehicle-, oMSC and sMSC-treated groups (*p <0.05). Error bars: SEM.

(**d**) In vivo activity of layer 2/3 neurons located in the vicinity of amyloid plaques in the cortex of 7-8-month-old APP23xPS45 mice after INA of vehicle or o/sMSC (2x application of 1×10^6 cells, n=5 mice per group). Left panel: Neurons classified based on the frequency of their spontaneous Ca^{2+} transients as silent (0-0.25 transients/min), normal (0.26-4 transients/min), and hyperactive (>4 transients/min) [31]. Pie charts show fractions of hyperactive (red), normal (green) and silent (blue) cells. The relative fractions of different cell types are significantly different (Chi-square test. Vehicle *vs.* oMSC: p=0.0006, ChiSquare=14.95, df=2; vehicle *vs.* sMSC: p<0.0001, ChiSquare=31.83, df=2; oMSC *vs.* sMSC: p=0.034, ChiSquare=6.79, df=2). Right panel: Cumulative histogram showing frequency distribution of Ca^{2+} transients recorded from neurons close to amyloid plaques after INA of vehicle (225 cells), oMSC (285 cells), and sMSC (310 cells). oMSC and sMSC treatment shifted the frequency distribution significantly towards lower values, and therefore reduced pathological hyperactivity in cortical neurons (Kolmogorov-Smirnov-test. Vehicle *vs.* oMSC: p<0.0001, D=0.204; Vehicle *vs.* sMSC: p<0.0001, D=0.336; oMSC *vs.* sMSC: p=0.0002, D=0.173).

(**e**) Analysis of indicated protein levels by V-plex® analysis (n=5-8 per group; individual samples were collectively analysed by V-plex®) and mRNA levels by qPCR (n=4-5 per group; individual samples collectively analysed for the respective targets) after INA of oMSC and sMSC. IL-12 and IFNγ were barely detectable (data not shown). ANOVA with Bonferroni's multiple comparisons test was used to compare vehicle-, oMSC and sMSC-treated groups (*p <0.05; ***p <0.001). Error bars: SEM. IL, interleukin; NEP, neprilysin. (For interpretation of the references to color in this figure legend, the reader is referred to the web version of this article.)

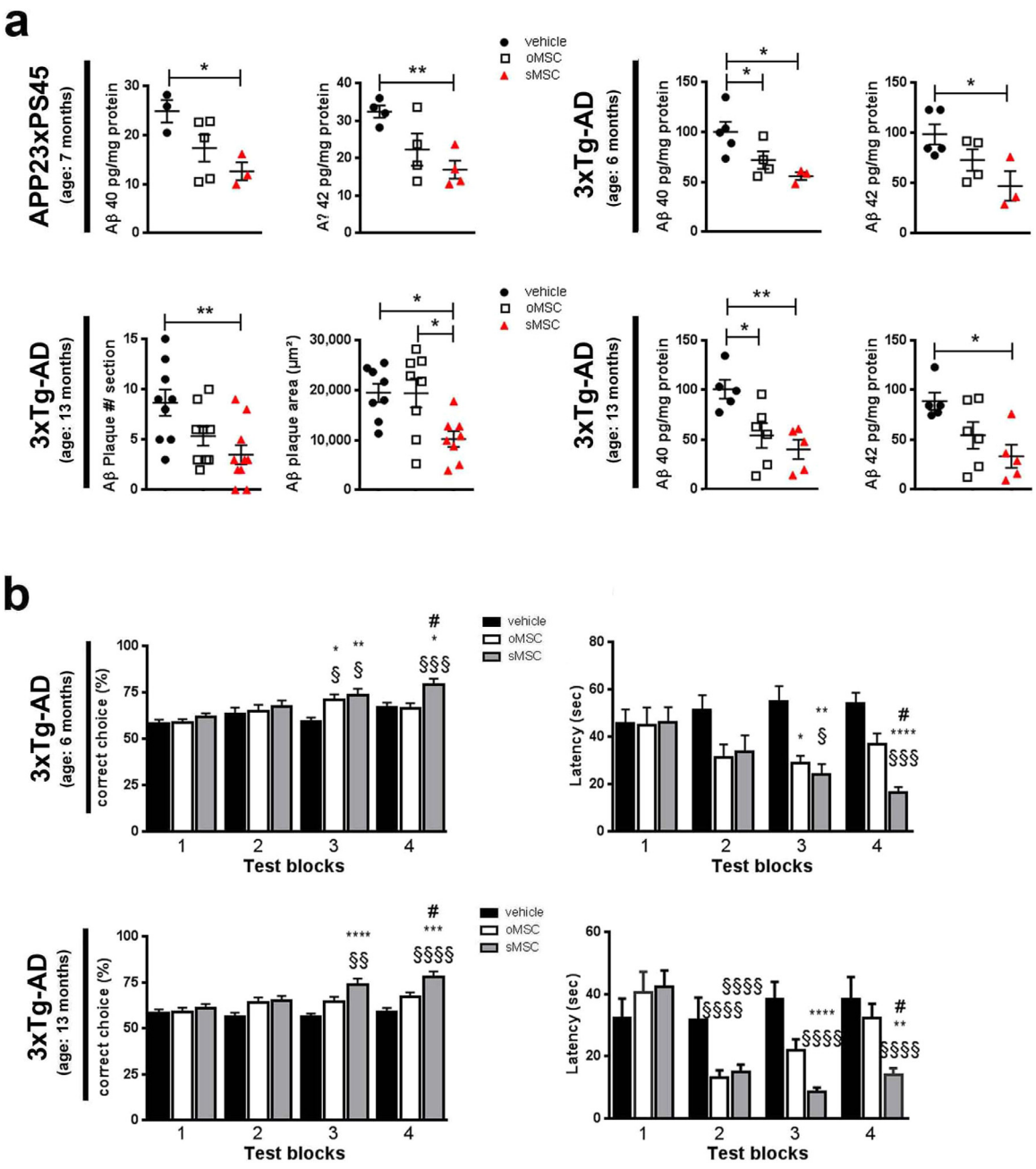

Fig. 7. Aβ pathology and memory deficits after intranasal oMSC or sMSC treatment in transgenic AD mice

(**a**) Human Aβ 40 and 42 quantified by ELISA in 7-month-old APP23/PS45 mice (n=4 per group), 6-month-old 3xTg-AD mice (n=5 per group) and 13-months-old 3xTg-AD mice (n=5 per group) after INA of o/sMSC (2x application of 1×10^6 cells). Aβ plaque number and cumulative area in the hippocampi of 13-month-old 3xTg-AD mice (n=3 per group) after INA of o/sMSC (2x application of 1×10^6 cells). Number of plaques and cumulative area per brain section quantified from 9-10 brain sections per animal using the APP/Aβ antibody 6E10, each data point represents plaque number or plaque area calculated per section. Each column represents 8-10 data points obtained from 9-10 sections. To compare vehicle-, oMSC and sMSC-treated groups ANOVA with Bonferroni's multiple comparisons test was used (*p <0.05; **p <0.01). Error bars: SEM.

(**b**) Performance in T-maze of 6- and 13-month-old 3xTg-AD mice (n=8 per group) prior (test block 1) and after (test blocks 2-4) INA of o/s MSC (2x application of 1×10^6 cells) shown in test blocks with 4 consecutive test days in each block. Experiments performed once with 6-month-old mice, and twice in 13-month-old mice. The test blocks 2-4 were performed from day 13 to day 28 after INA. In the "correct choice" assessment, each bar represents 32 values of correct choice percentages out of 6 runs on 4 consecutive days of one test block assessed from 8 animals per group. In the latency assessment each bar represents 24-42 data points of latency to reach the correct arm on the last day of each test block from 6-8 mice out of 8 mice analysed. #-comparison between oMSC and sMSC, *-comparison between o/sMSC and PBS (vehicle) group, §-comparison of the respective treatment group in test blocks after INA *vs.* test block 1 (for instance oMSC of test block 1 *vs.* oMSC in test blocks 2-4). ANOVA with Bonferroni's multiple comparisons test was used (*p <0.05; **p <0.01; ***p<0.001). Error bars: SEM.

analysis of the PDPN protein (Fig. 2**c**). Further loss- and gain-of-function experiments revealed a pivotal role of PDPN in SC motility. Specifically, the siRNA-mediated *PDPN* knockdown in sMSC decreased their migration potential down to the oMSC level (Fig. 3**a**), while transient overexpression of PDPN in oNSC and oMSC, as confirmed by flow cytometry (**Supplementary Fig. 3**), increased their migration capacities (**Fig.3b**).

To evaluate the applicability of PDPN engineering for SC therapies, we overexpressed PDPN in oncolytic adenovirus (Ad-Delo3-RGD) [9] infected NSC to enhance their migration to and thus the oncovirolysis of glioma cells. Using an in vitro transwell migration assay, either control or PDPN overexpressing, Ad-Delo-RGD or mock-treated NSC were allowed to migrate towards the conditioned medium from LNT-229 glioma cells. The migration of control cells was slightly, but not

significantly reduced by virus infection, while PDPN overexpressing cells migrated better than control cells, independently from virus infection (**Fig. 4a**). Migrated cells were thereafter co-cultured with eGFP-labelled LNT-229 ^{GFP} glioma cells to demonstrate oncolysis by the NSC- or sNSC-released OV progeny (**Fig. 4b**). While non-infected NSC (with and without PDPN overexpression) could not influence the rapid growth of glioma cells (**Fig. 4c**), PDPN overexpressing Ad-Delo3-RGD-infected NSC killed eGFP-labelled LNT-229^{GFP} cells more efficiently on day 5 and 7 in co-culture compared to Ad-Delo3-RGD-infected NSC without PDPN overexpression (**Fig. 4d**).

3.2. Highly migrating SC subpopulations show superior therapeutic efficacy in transgenic AD models

The delivery efficacy of oMSC and sMSC was evaluated after INA in two mouse models of AD: the APP23xPS45 and the triple transgenic (3xTg-AD) models. The highest density of both oMSC and sMSC appeared in the dentate gyrus (DG) in close vicinity to APP/Aβ positive host cells and Aβ plaques (**Fig. 5a**). Notably, significantly greater numbers of sMSC were observed in different brain areas of 3xTg-AD mice compared to oMSC (**Fig. 5b**). This is likely due to their superior migration capacities as in vivo proliferation of both populations was generally low (**Fig. 5c**).

Further, sMSC's stimulation of neurogenesis shown by doublecortin (DCX) (**Fig. 6a**), survival of DG neurons (**Fig. 6b**) and synaptic integrity reflected by synaptophysin (**Fig. 6c**) were generally greater than that of oMSC. The expression of synapsin (**Supplementary Fig. 4a**) and PSD95 (**Fig. 6e**) was not significantly changed in either of the cell treated groups.

A landmark study identified neuronal hyperactivity as a functional hallmark of AD [31]. In vivo analyses demonstrated the superior ability of sMSC to reduce cortical hyperactivity compared to oMSCs (**Fig. 6d**). Inflammation is also a crucial factor in AD pathogenesis [32]. Both sMSC and oMSC decreased IL-6 protein levels in the brain, while *IL-6* mRNA remained unchanged (**Fig. 6e**). Interestingly, INA specifically of sMSC increased TNFα, while IL-10 protein was highly variable along with enhanced *IL-10* mRNA in both sMSC and oMSC populations (**Fig. 6e**). The brain content of Iba-1 positive microglia and CD11b/F4/80 and CD11b/MHCII positive macrophages remained unchanged (**Supplementary Fig. 4b–d**). Altogether, we found that enhancing the migratory capacity of MSC increased their accumulation in specific brain regions, and by doing so significantly enhanced the survival of neurons in the dentate gyrus and increased hippocampal neurogenesis as well as synaptic activity in 3xTg-AD mice.

We next analysed Aβ plaque pathology by quantifying the expression of the Aβ degrading enzyme neprilysin (NEP), soluble Aβ42 and Aβ40, as well as Aβ plaque number and areas. Only sMSC were effective enhancers of *NEP* mRNA expression (**Fig. 6e**). They also showed a stronger potency to reduce Aβ plaques and soluble Aβ fragments, most clearly in the triple transgenic AD model where only sMSC had an effect and significantly reduced Aβ plaque area by an average of 47±12 % (**Fig. 7a).**

To test the functional relevance of improved in vivo MSC homing to the areas affected by Aβ pathology, we assessed spatial working memory in the 3xTg-AD mice using the forced choice alternation T-maze assay (Fig. **7b**). In both 6- and 13-month old 3xTg-AD mice, 19-22 days after INA of either vehicle, oMSC or sMSC, sMSC led to a significantly better performance and shorter latency to find the correct arm than the oMSC group (test block 4 in **Fig. 7b**). Of note, improved memory was not correlated to choline acetyltransferase (ChAT) expression or to the brain content of trophic factors IGF-1, GDNF, VEGF and NGF in the cell-treated groups (**Supplementary Fig. 4e,f**). The number of BrdU-positive cells in the brains of 3xTg-AD mice remained unchanged in vehicle- vs. both cell-treated groups (**Supplementary Fig. 4g**)

3.3. Targeted homing of highly migrating SC is applicable in an orthotopic model of glioblastoma

As SC show tumour tropism [6], we finally assessed the MSC's trans-hemispheric migration rate towards previously implanted GBM cells to validate their in vivo migration capacities. All treatment groups (vehicle, oMSC and sMSC) revealed nearly equal tumour growth and tumour volume assessed by MRI (**Fig. 8a, Supplementary Fig. 5**). Significantly more sMSC than oMSC migrated to the tumours than oMSC (**Fig. 8b**) and were detectable within the tumour tissue (arrows in **Fig. 8c**). This provides further evidence for their superior in vivo migration capacities and confirms migration through tissue as a relevant mechanism for SC therapies' efficacy.

4. Discussion

Our data show that targeting SC homing by selecting highly migrating subpopulations can enhance SC therapeutic efficacy in brain pathologies including tumour and neurodegeneration. Selection of cells based on their migration properties provides a simple procedure without genetic engineering of cell candidates. However, the success of this method requires the presence of an expandable

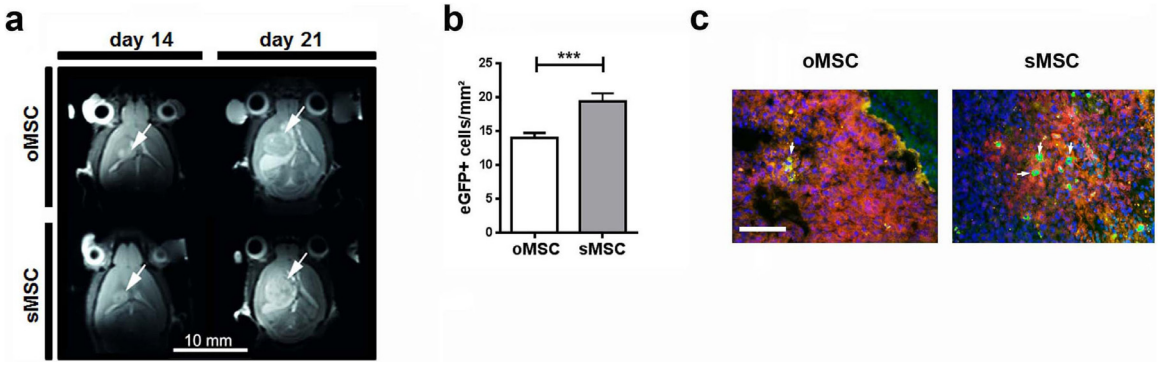

Fig. 8. In vivo intracerebral administration of oMSC and sMSC in an orthotopic model of glioblastoma

(**a**) GL-261-Luc (1×10^5 cells) were injected into the brain of C57BL/6 mice and a T2-weighted MR-anatomy was acquired 14 and 21 days post injection. eGFP+ oMSC or sMSC (1×10^5 cells) were injected into the contralateral side on day 15 after intracerebral injection of GL-261-Luc cells. Tumours are indicated with arrows.

(**b**) Quantification of eGFP+ oMSC and sMSC in the tumour area 7 days after intracerebral injection of eGFP-MSC (n=7 per group). The columns represent 150-180 data points obtained from 20-25 sections per mouse brain. The numbers of eGFP+ oMSC and sMSC were compared by two-tailed t-test (***$p < 0.001$); Error bars: SEM.

(**c**) eGFP+ oMSC and sMSC (green) highlighted with arrows in the GL-261-Luc (red) tumour area 7 days after intracerebral injection of 1×10^5 eGFP+ o/sMSC into the contralateral hemisphere. Scale bar: 100 μm. (For interpretation of the references to color in this figure legend, the reader is referred to the web version of this article.)

amount of highly migrating subpopulation(s) among the original cell preparation. For those primary cells and cell lines that do not meet this criterion, the generation of PDPN (over)expressing cells may help to improve cell motility. This notion is supported by our discovery identifying PDPN as one of the factors involved in the high migration capacity of SC.

PDPN, a transmembrane mucin-like protein released within EVs [33], plays a critical role in organ development, cell motility and migration [34,35]. On the other hand, PDPN is also associated with tumour cell invasiveness and migration including glioblastoma [36,37]. However, we found no increased proliferation of transplanted sMSC (highly expressing PDPN, **Fig. 5c**) or host brain cells (**Supplementary Fig. 4g**) in the 3xTg-AD mice. PDPN is also a regulator of synaptic plasticity and hippocampus-dependent learning and memory in mice [38]. Therefore, PDPN release by transplanted (PDPN overexpressing) SC may both increase their migration and alleviate synaptic dysfunction and memory deficits in AD.

Origin-specific difference in PDPN expression has been reported for MSC isolated from the bone marrow or umbilical cord [39]. PDPN-dependent migration of MSC is suggested to be regulated by GTPase Rac-1 [35] which is also known to mediate tumour cell migration [40]. Our data reveal PDPN-dependent motility and migration of highly migrating subpopulations across two different classes of SC (MSC and NSC). Whether the sole engineering of PDPN will lead to the therapeutic efficacy of SC equipotent to that of naturally programmed highly migrating subpopulations will be a matter of future investigations in a roadmap for translation of this concept into clinical applications.

Comparative analyses of EV release and trophic features of oMSC and sMSC in vitro and in the 3xTg-AD model, including their capacities to release and/or regulate trophic factors levels in the host tissue, suggest that the enrichment of cell transplants with highly migrating cell population(s) does not affect their regenerative features. Moreover, the transcriptome signature that distinguished the sMSC from the oMSC specifically comprised cell migration and/or adhesion but not trophic factors genes. This suggests the content of highly migrating cells within SC therapeutics as a major mechanism of SC therapies' efficacy.

Naïve MSC may promote tumour growth in vivo [41]. Therefore, we analysed the tumour sizes in our GBM model after o/sMSC application by MRI. As no tumour size differences were detected (**Supplementary Fig. 5**), we conclude that sMSC did not feature greater tumour promoting risks than oMSC. Further, the previously well-described tumour tropism of oncolytic SC [6] may be enhanced by selecting highly migrating SC subpopulations, thus opening new avenues for applying this concept to CBT in oncology.

Our in vivo studies highlight the impact of improved sMSC migration and homing on the hallmarks of AD-like pathology as demonstrated by their superior efficacy for improving spatial memory and reducing cortical neuronal hyperactivity as well as on the processes regulating the extent of AD pathology comprising inflammation, neuronal death, neurogenesis, Aβ deposition and degradation. Moreover, we show that superior efficacy does not require enhanced in vivo graft cell proliferation. INA of highly migrating SC subpopulations combines the advantages of non-invasiveness and greater efficacy, where poor cell transplant survival might become relevant in Alzheimer's dementia [42].

At first site intranasal delivery in humans might seem to be connected with obstacles such as the longer distance that cells should traverse from the nasal mucosa to the brain. However, a closer look at the mechanisms and pathways of intranasal cell delivery discovered by us 11 years ago, reveals that cells use nearly the same delivery mechanisms (besides active migration) as described for peptides and growth factors [43]. This is evidenced by their rapid appearance within the brain, just a few hours after administration as shown by us for MSC [10,44] or within a day as reported by other groups for NSC [45,46]. Hereby, it is suggested that besides active migration promoting the cell distribution within the brain, a complex of tools such as bulk flow, vessel pulsation when the cells move along perivascular spaces, as well as nose-to-brain interconnection of lymphatic and cerebrospinal fluid systems contribute to their rapid entry into the brain and further distribution to different brain areas [43,44]. Moreover, the comparison of the cribriform plate's anatomy in humans and rodents, which is the first rigid mechanical barrier for cells on the way from the nasal epithelium to the brain [47–49], allow us to suggest that the larger area and size of the cribriform plate foramina in humans would facilitate the migration of cells through these narrow openings when compared to that of rodents. Another issue that may impact transnasal delivery of cells to the brain is their long persistence, i.e. hours or up to several days, within the nasal cavity [44,50] which is highly equipped with immunocompetent cells due to continuous exposure to antigenic stimuli. However, this notion is counterbalanced by the fact that human MSC and NSC can reach the brain after intranasal administration in immunocompetent rodent models of brain disorders [12,51]. Moreover, intranasally administered human MSC derived from clinical-grade human iPSC line were shown to provide greater protection than corticosteroids against allergic airways disease in mice [52]. Intranasally applied NSC have also been successfully delivered to the brain in a model with strong local, i.e. within the central nervous system (CNS), and systemic immune response to disease induction, such as multiple sclerosis [53]. These findings suggest that immunomodulatory properties of SC allow them to escape destruction by immune cells in the nasal cavity and in the brain to a sufficient extent for fulfilment of their therapeutic effects. For those SC candidates that are more susceptible to the local immune response, immunosuppressive approaches [54] or priming tools such as in vitro preconditioning can be suggested [55].

Another important aspect in development of cell therapies for CNS disorders is the verification of successful SC delivery by in vivo imaging approaches. Besides superparamagnetic iron oxide–based agents or fluorinated tracer based tracking by magnetic particle imaging (MPI) or MRI, PET/SPECT with direct radioactive labelling or with reporter gene transfection of cells are suggested to be non-invasive clinically translatable methods for cell detection in the future [56].

Of note, the strategy of using highly migrating SC is applicable not only for INA, but for all other administration routes when it comes to treatment of diseases with multifocal brain pathology (such as, AD or multiple sclerosis) or when the diseased areas are far away from the site of cell administration. Future development of this strategy may include testing of surgically or systemically applied highly migrating SC in animals larger than rodents such as canine models of brain tumours or AD [57,58]. For testing of highly migrating SC by intranasal administration route significant differences in gross anatomy of the nasal cavity and olfactory epithelium of macrosmatic (rodents, dogs) and microsmatic species (primates, humans) should be taken into consideration [43,59]. Recent advances in the development of non-human primate models of neurodegenerative disorders, including AD [60–62] enables future testing of intranasal highly migrating SC in species sharing the closest relationship with humans as the next step towards translation of this delivery route into the clinical use.

The concept of SC migration heterogeneity described here demonstrates the high impact of SC motility on their therapeutic properties. Thus, future production of migration properties-based customized cellular grafts may represent the game-changing strategy in SC therapies of brain and potentially other organs' disorders.

4.1. Data sharing

The microarray data requires controlled access which will be granted to qualified investigators for appropriate use. Terms and

conditions are listed in the associated Data Access Agreement (DAA). The DAA must be signed by the applicant and the relevant institutional or administrative authority. If applications include a named collaborator, a separate DAA must be signed. In addition, applicants will be asked to complete and sign a Data Access Form (including a brief summary of the proposal, a full list of applicants´ and co-applicants´ names, and the data storage), to enable the responsible Data Access Committee to assess if the intended usage complies to the consents. Details on how to request access to this dataset is specified on the EGA homepage (https://ega-archive.org) under the study accession number EGAS00001002478 and the DAC accession number EGAC00001000667.

HB1.F3 cell line (RRID: CVCL_LJ44) is available upon written request to Prof. Hong J. Lee, College of Medicine and Medical Research Institute, Chungbuk National University, Cheongju, Chungbuk, Republic of Korea; and signed material transfer agreement. Study-specific primary cell material can be provided upon availability and written request to the corresponding authors and signed material transfer agreement. All other materials used in this study are commercially available.

Funding sources

This work was supported in part by the Robert Bosch Stiftung (Stuttgart, Germany) given to M.S., E. Schaeffeler and S.W., by the IZEPHA grant given to L.D. The funders had no role in study design, data collection, data analysis, interpretation or writing of the report.

Authors` contributions

R.S. and L.D. designed the research, analysed the data and wrote the manuscript. A.K., A.L., M.B., A.S., B.B., N.A., M.A-A., M.A.K, C.C., U. N., S.B-H., J.N., S.W., K. Barth, K.M., G. Siegel, G. Spohn, and E. Schaeffeler performed the experiments, analysed the data and reviewed the manuscript. O.G., W.H.F., M.S., C.H.G., H-P.W., E-M.A., C.D.C., E.S., D.M. H, T.R.D. and H.N. discussed the results and reviewed the manuscript. H. J. L. and S. U. K. provided the HB1.F3 cell line and reviewed the manuscript. The authors (L.D., R.S., M.S., and C.H.G.) and the University of Tübingen filed patent applications for the selection of highly migrating cell subpopulations (US14/634,501, US14/634,484, PCT/EP2016/054055, DE102012107879, EP2888348). All authors read and approved the final version of the manuscript.

Declaration of Competing Interest

Dr. Danielyan reports grants from IZEPHA, during the conduct of the study. Prof.. Schwab, Dr. Schaeffeler and Dr. Winter report grants from Robert Bosch Stiftung (Stuttgart, Germany), during the conduct of the study. Dr. Danielyan, Dr. Schäfer, Prof. Gleiter and Prof. Schwab have a patent US14/634,501, US14/634,484, PCT/EP2016/054055, DE102012107879, EP2888348 pending. All other authors have no competing interests.

Acknowledgements

Authors wish to thank Barbara Proksch, Andreas Behring, Michael Glaser, Andrea Jarmuth, Ursula Waldherr, and Claudia Mueller for technical assistance, as well as Life Science Editors for editorial assistance. Authors acknowledge support by the Open Access Publishing Fund of University of Tübingen.

Supplementary materials

Supplementary material associated with this article can be found, in the online version, at doi:10.1016/j.ebiom.2020.102989.

References

[1] Fu Liu, Halim Ju, Luo Song. Mesenchymal stem cell migration and tissue repair. Cells 2019;8:784.
[2] Mendonça LS, Onofre I, Miranda CO, Perfeito R, Nóbrega C, de Almeida LP. Stem cell-based therapies for polyglutamine diseases. Adv. Exp. Med. Biol. 2018;1049:439–66.
[3] Terunuma A, Ashiba K, Takane T, Sakaguchi Y, Terunuma H. Comparative transcriptomic analysis of human mesenchymal stem cells derived from dental pulp and adipose tissues. J Stem Cells Regen Med 2019;15:8–11.
[4] Severe N, Karabacak NM, Gustafsson K, Baryawno N, Courties G, Kfoury Y, et al. Stress-induced changes in bone marrow stromal cell populations revealed through single-cell protein expression mapping. Cell Stem Cell 2019;25:570–583.e7.
[5] Majore I, Moretti P, Hass R, Kasper C. Identification of subpopulations in mesenchymal stem cell-like cultures from human umbilical cord. Cell Commun Signal 2009;7.
[6] Krueger TEG, Thorek DLJ, Denmeade SR, Isaacs JT, Brennen WN. Concise review: mesenchymal stem cell-based drug delivery: the good, the bad, the ugly, and the promise. Stem Cells Transl Med 2018;7:651–63.
[7] Shetty AK, Rao MS, Hattiangady B. Behavior of hippocampal stem/progenitor cells following grafting into the injured aged hippocampus. J Neurosci Res 2008;86:3062–74.
[8] Matchynski-Franks JJ, Pappas C, Rossignol J, Reinke T, Fink K, Crane A, et al. Mesenchymal stem cells as treatment for behavioral deficits and neuropathology in the 5xFAD mouse model of Alzheimer's disease. Cell Transp 2016;25:687–703.
[9] Mantwill K, Naumann U, Seznec J, Girbinger V, Lage H, Surowiak P, et al. YB-1 dependent oncolytic adenovirus efficiently inhibits tumor growth of glioma cancer stem like cells. J Transl Med 2013;11.
[10] Danielyan L, Schäfer R, von Ameln-Mayerhofer A, Bernhard F, Verleysdonk S, Buadze M, et al. Therapeutic efficacy of intranasally delivered mesenchymal stem cells in a rat model of Parkinson disease. Rejuvenation Res 2011;14:3–16.
[11] Danielyan L, Beer-Hammer S, Stolzing A, Schäfer R, Siegel G, Fabian C, et al. Intranasal delivery of bone marrow-derived mesenchymal stem cells, macrophages, and microglia to the brain in mouse models of Alzheimer's and Parkinson's disease. Cell Transp 2014;23:123–39.
[12] Donega V, Nijboer CH, Braccioli L, Slaper-Cortenbach I, Kavelaars A, Van Bel F, et al. Intranasal administration of human MSC for ischemic brain injury in the mouse: In vitro and in vivo neuroregenerative functions. PLoS One 2014;9.
[13] Wei N, Yu SP, Gu X, Taylor TM, Song D, Liu XF, et al. Delayed intranasal delivery of hypoxic-preconditioned bone marrow mesenchymal stem cells enhanced cell homing and therapeutic benefits after ischemic stroke in mice. Cell Transp 2013;22:977–91.
[14] Fransson M, Piras E, Wang H, Burman J, Duprez I, Harris RA, et al. Intranasal delivery of central nervous system-retargeted human mesenchymal stromal cells prolongs treatment efficacy of experimental autoimmune encephalomyelitis. Immunology 2014;142:431–41.
[15] Yu-Taeger L, Stricker-Shaver J, Arnold K, Bambynek-Dziuk P, Novati A, Singer E, et al. Intranasal administration of mesenchymal stem cells ameliorates the abnormal dopamine transmission system and inflammatory reaction in the R6/2 Mouse model of Huntington disease. Cells 2019;8:595.
[16] Assmus B, Leistner DM, Schächinger V, Erbs S, Elsässer A, Haberbosch W, et al. Long-term clinical outcome after intracoronary application of bone marrow-derived mononuclear cells for acute myocardial infarction: Migratory capacity of administered cells determines event-free survival. Eur Heart J 2014;35:1275–83.
[17] Bartolucci J, Verdugo FJ, González PL, Larrea RE, Abarzua E, Goset C, et al. Safety and efficacy of the intravenous infusion of umbilical cord mesenchymal stem cells in patients with heart failure: a phase 1/2 randomized controlled trial (RIMECARD trial [Randomized clinical trial of intravenous infusion umbilical cord mesenchymal. Circ Res 2017;121:1192–204.
[18] Ottoboni L, von Wunster B, Martino G. Therapeutic plasticity of neural stem cells. Front Neurol 2020;11.
[19] Huang B, Tabata Y, Gao JQ. Mesenchymal stem cells as therapeutic agents and potential targeted gene delivery vehicle for brain diseases. J Control Release 2012;162:464–73.
[20] Shah K. Stem cell-based therapies for tumors in the brain: are we there yet? Neuro Oncol 2016;18:1066–78.
[21] Lo Furno D, Mannino G, Giuffrida R. Functional role of mesenchymal stem cells in the treatment of chronic neurodegenerative diseases. J Cell Physiol 2018;233:3982–99.
[22] Siegel G, Kluba T, Hermanutz-Klein U, Bieback K, Northoff H, Schäfer R. Phenotype, donor age and gender affect function of human bone marrow-derived mesenchymal stromal cells. BMC Med 2013;11.
[23] Lindl T, Lewandowski B, Schreyögg S, Stäudte A. An evaluation of the in vitro cytotoxicities of 50 chemicals by using an electrical current exclusion method versus the neutral red uptake and MTT assays. ATLA Altern Lab Anim 2005;33:591–601.
[24] Avci-Adali M, Behring A, Keller T, Krajewski S, Schlensak C, Wendel HP. Optimized conditions for successful transfection of human endothelial cells with in vitro synthesized and modified mRNA for induction of protein expression. J Biol Eng 2014;8.
[25] Höring E, Harter PN, Seznec J, Schittenhelm J, Bühring HJ, Bhattacharyya S, et al. The “go or grow” potential of gliomas is linked to the neuropeptide processing enzyme carboxypeptidase E and mediated by metabolic stress. Acta Neuropathol 2012;124:83–97.

[26] Irizarry RA, Hobbs B, Collin F, Beazer-Barclay YD, Antonellis KJ, Scherf U, et al. Exploration, normalization, and summaries of high density oligonucleotide array probe level data. Biostatistics 2003;4:249–64.
[27] R Core Team. R: A language and environment for statistical computing. Vienna, Austria: R Foundation for Statistical Computing; 2018. URL https://www.R-project.org/.
[28] Lappalainen I, Almeida-King J, Kumanduri V, Senf A, Spalding JD, Ur-Rehman S, et al. The European genome-phenome archive of human data consented for biomedical research. Nat Genet 2015;47:692–5.
[29] Stosiek C, Garaschuk O, Holthoff K, Konnerth A. In vivo two-photon calcium imaging of neuronal networks. Proc Natl Acad Sci U S A 2003;100:7319–24.
[30] Garaschuk O, Milos RI, Konnerth A. Targeted bulk-loading of fluorescent indicators for two-photon brain imaging in vivo. Nat Protoc 2006;1:380–6.
[31] Busche MA, Eichhoff G, Adelsberger H, Abramowski D, Wiederhold KH, Haass C, et al. Clusters of hyperactive neurons near amyloid plaques in a mouse model of Alzheimer's disease. Science 2008;321(80-):1686–9.
[32] Heneka MT, Carson MJ, El Khoury J, Landreth GE, Brosseron F, Feinstein DL, et al. Neuroinflammation in Alzheimer's disease. Lancet Neurol 2015;14:388–405.
[33] Carrasco-Ramírez P, Greening DW, Andrés G, Gopal SK, Martín-Villar E, Renart J, et al. Podoplanin is a component of extracellular vesicles that reprograms cell-derived exosomal proteins and modulates lymphatic vessel formation. Oncotarget 2016;7:16070–89.
[34] Astarita JL, Acton SE, Turley SJ. Podoplanin: Emerging functions in development, the immune system, and cancer. Front Immunol 2012;3.
[35] Ward LSC, Sheriff L, Marshall JL, Manning JE, Brill A, Nash GB, et al. Podoplanin regulates the migration of mesenchymal stromal cells and their interaction with platelets. J Cell Sci 2019;132.
[36] Grau SJ, Trillsch F, Tonn JC, Goldbrunner RH, Noessner E, Nelson PJ, et al. Podoplanin increases migration and angiogenesis in malignant glioma. Int J Clin Exp Pathol 2015;8:8663–70.
[37] Dang Q, Liu J, Li J, Sun Y. Podoplanin: a novel regulator of tumor invasion and metastasis. Med Oncol 2014;31:1–6.
[38] Cicvaric A, Yang J, Krieger S, Khan D, Kim EJ, Dominguez-Rodriguez M, et al. The brain-tumor related protein podoplanin regulates synaptic plasticity and hippocampus-dependent learning and memory. Ann Med 2016;48:652–68.
[39] Sheriff L, Alanazi A, Ward LSC, Ward C, Munir H, Rayes J, et al. Origin-specific adhesive interactions of mesenchymal stem cells with platelets influence their behavior after infusion. Stem Cells 2018;36:1062–74.
[40] Sanz-Moreno V, Gadea G, Ahn J, Paterson H, Marra P, Pinner S, et al. Rac activation and inactivation control plasticity of tumor cell movement. Cell 2008;135:510–23.
[41] Melzer C, von der Ohe J, Lehnert H, Ungefroren H, Hass R. Cancer stem cell niche models and contribution by mesenchymal stroma/stem cells. Mol Cancer 2017;16.
[42] Ruzicka J, Kulijewicz-Nawrot M, Rodrigez-Arellano JJ, Jendelova P, Sykova E. Mesenchymal stem cellreserve working memory in the 3xTg-AD mousodel of Alzheimer's disease. Int J Mol Sci 2016;17.
[43] Lochhead JJ, Thorne RG. Intranasal delivery of biologics to the central nervous system. Adv Drug Deliv Rev 2012;64:614–28.
[44] Danielyan L, Schäfer R, von Ameln-Mayerhofer A, Buadze M, Geisler J, Klopfer T, et al. Intranasal delivery of cells to the brain. Eur J Cell Biol 2009;88:315–24.
[45] Reitz M, Demestre M, Sedlacik J, Meissner H, Fiehler J, Kim SU, et al. Intranasal delivery of neural stem/progenitor cells: a noninvasive passage to target intracerebral glioma. Stem Cells Transl Med 2012;1:866–73.
[46] Ye Q, Wu Y, Wu J, Zou S, Al-Zaazaai AA, Zhang H, et al. Neural stem cells expressing bFGF reduce brain damage and restore sensorimotor function after neonatal Hypoxia-Ischemia. Cell Physiol Biochem 2018;45:108–18.
[47] Edwards B, Wang JM, Iwanaga J, Loukas M, Tubbs RS. Cranial nerve foramina part i: a review of the anatomy and pathology of cranial nerve foramina of the anterior and middle fossa. Cureus 2018.
[48] Kalmey JK, Thewissen JGM, Dluzen DE. Age-related size reduction of foramina in the cribriform plate. Anat Rec 1998;251:326–9.
[49] Norwood JN, Zhang Q, Card D, Craine A, Ryan TM, Drew PJ. Anatomical basis and physiological role of cerebrospinal fluid transport through the murine cribriform plate. Elife 2019;8.
[50] Galeano C, Qiu Z, Mishra A, Farnsworth SL, Hemmi JJ, Moreira A, et al. The route by which intranasally delivered stem cells enter the central nervous system. Cell Transplant 2018;27:501–14.
[51] Ji G, Liu M, Zhao XF, Liu XY, Guo QL, Guan ZF, et al. NF-κB signaling is involved in the effects of intranasally engrafted human neural stem cells on neurofunctional improvements in neonatal rat hypoxic-ischemic encephalopathy. CNS Neurosci Ther 2015;21:926–35.
[52] Royce SG, Mao W, Lim R, Kelly K, Samuel CS. iPSC- and mesenchymoangioblast-derived mesenchymal stem cells provide greater protection against experimental chronic allergic airways disease compared with a clinically used corticosteroid. FASEB J 2019.
[53] Wu S. Intranasal delivery of neural stem cells: a CNS-specific, non-invasive cell-based therapy for experimental autoimmune encephalomyelitis. J Clin Cell Immunol 2013;04.
[54] Diehl R, Ferrara F, Müller C, Dreyer AY, McLeod DD, Fricke S, et al. Immunosuppression for in vivo research: State-of-The-Art protocols and experimental approaches. Cell Mol Immunol 2017.
[55] Sart S, Ma T, Li Y. Preconditioning stem cells for in vivo delivery. Biores Open Access 2014;3:137–49.
[56] Bulte JWM, Daldrup-Link HE. Clinical tracking of cell transfer and cell transplantation: trials and tribulations. Radiology 2018;289:604–15.
[57] Hicks J, Platt S, Kent M, Haley A. Canine brain tumours: a model for the human disease? Vet Comp Oncol 2017;15:252–72.
[58] Schmidt F, Boltze J, Jäger C, Hofmann S, Willems N, Seeger J, et al. Detection and quantification of β-Amyloid, Pyroglutamyl Aβ, and Tau in Aged Canines. J Neuropathol Exp Neurol 2015;74:912–23.
[59] Chamanza R, Wright JA. A review of the comparative anatomy, histology, physiology and pathology of the nasal cavity of rats, mice, dogs and non-human primates. relevance to inhalation toxicology and human health risk assessment. J Comp Pathol 2015;153:287–314.
[60] Chen ZZ, Niu YY. Stem cell therapy for Parkinson's disease using non-human primate models. Zool Res 2019;40:349–57.
[61] Van Dam D, De Deyn PP. Non human primate models for Alzheimer's disease-related research and drug discovery. Expert Opin Drug Discov 2017;12:187–200.
[62] Peng Z, Zhang L, Wang H, He X, Peng X, Zhang Q, et al. Experimental Autoimmune Encephalomyelitis (EAE) Model of Cynomolgus Macaques Induced by Recombinant Human MOG1-125 (rhMOG1-125) Protein and MOG34-56 Peptide. Protein Pept Lett 2018;24.